A low δ^7Li lower crustal component: evidence from an alkalic intraplate volcanic series (Chaîne des Puys, French Massif Central).

Cédric Hamelin[a], Hans-Michael Seitz[b], Jean-Alix Barrat[a], Laure Dosso[c], René C. Maury[a] and Marc Chaussidon[d]

[a] *UEB, Université de Brest, CNRS UMR 6538, I.U.E.M., place N. Copernic, 29280 Plouzané Cedex, France.*

[b] *Institut für Geowissenschaften, Universität Frankfurt, 1 Altenhöferallee, 60438 Frankfurt, Germany.*

[c] *CNRS UMR 6538, IFREMER, BP70, 29280 Plouzané, France*

[d] *CRPG-CNRS UPR 2300, 15 rue Notre-Dame des Pauvres, 54501 Vandoeuvre-les-Nancy Cedex, France.*

Submitted to Chemical Geology

Abstract

The intraplate volcanic suite of the Chaîne des Puys (French Massif Central) shows a complete petrologic range, from alkali basalts to trachytes. The significant variations of trace elements and radiogenic isotopes along the series strongly support the occurrence of crustal assimilation associated with fractional crystallization (AFC). The least contaminated basalts are clearly related to a HIMU-type reservoir ($^{206}Pb/^{204}Pb > 19.6$; $^{87}Sr/^{86}Sr < 0.7037$; $\varepsilon_{Nd} > +4$). The behavior of radiogenic isotopes suggests that the most likely crustal contaminants are meta-sediments located in the lower crust.

The Li isotopic compositions of the lavas range from high δ^7Li (> +7‰) in basalts to lighter values in more evolved lavas (down to $\delta^7Li \approx 0$‰). The mantle component, expressed in the least evolved lavas, has a heavy Li isotopic signature, in good agreement with previous δ^7Li measurements of OIB lavas with HIMU affinities. The evolution of Li isotopic compositions throughout the volcanic series is in agreement with the AFC model suggested by the Sr-Nd-Pb isotopic systems. Although the behavior of Li isotopes during assimilation processes is currently poorly constrained, our calculations suggest that at least a portion of the lower crust beneath the Chaîne des Puys is characterized by a light Li isotopic composition ($\delta^7Li < -5$‰).

Keywords: Li , Sr, Nd and Pb isotopes, lower crust, assimilation and fractional crystallization (AFC), HIMU, basalts, trachytes.

1. Introduction

The geochemistry of lithium isotopes has proven useful for a new look at a variety of Earth sciences problems in recent years. This alkali element has two stable isotopes, ^{6}Li and ^{7}Li, with a large relative mass difference (≅17%). Therefore, temperature-dependent isotopic fractionations, either equilibrium or kinetic, are anticipated for Li during natural processes. This property makes Li and its isotopes interesting for Earth science applications including the study of hydrothermal processes (Chan et al., 1992; Foustoukos et al., 2004), continental weathering rates (Huh et al., 1998; Huh et al., 2001; Rudnick et al., 2004), degassing events (Lentz et al., 2001; Beck et al., 2004), diffusion (Barrat et al., 2005; Lundstrom et al., 2005; Beck et al., 2006; Teng et al., 2006; Hamelin et al., 2007), metasomatic processes in peridotites (Wagner and Deloule, 2007; Rudnick and Ionov, 2007) and as a tracer of subducted oceanic crust in the mantle (Nishio et al., 2005; Elliot et al., 2006; Chan et al., 2009).

Although our understanding of Li isotope behavior has improved, our knowledge of the Li isotopic system within deep Earth reservoirs still remains quite rudimentary. In the case of the mantle reservoir, the end-members that have been identified using radiogenic isotopes are poorly constrained for the Li isotopic system. Most of the Ocean Island Basalts (OIB) show a range of $\delta^{7}Li$ that overlap the Mid Oceanic Ridge Basalts (MORB) range ($\delta^{7}Li \approx +3.4 \pm 1.4$‰, Tomascak et al., 2008). However, recent studies have reported significantly heavier Li isotopic composition for HIMU end-members ≈ +7‰ (Ryan and Kyle, 2004; Nishio et al., 2005; Aulbach et al., 2008; Chan et al., 2009). The Li isotopic signature of continental crust is also a matter of debate. This reservoir is vertically stratified in terms of its chemical composition and lithology. The upper part of the continental crust is well-known and exhibits a lighter Li isotopic composition (≈ 0‰) (Teng et al., 2004) than the upper mantle (e.g., Seitz et al., 2004). This isotopic signature is explained by ^{7}Li enrichment of river water relative to the original bed-rock and suspended load (Huh et al., 2001; Kisakurek et al., 2004). In contrast to the uppermost continental crust, the Li signature of the deeper crust (below 15 km depth) remains less-constrained. This reservoir has recently been investigated using samples from high-grade metamorphic

terranes and granulites-facies xenoliths carried in lavas (Teng et al., 2008). According to this study, the middle crust is estimated to be relatively homogeneous with δ^7Li average of +4.0‰ ±1.4 (1σ). Li isotopic composition of lower crustal xenoliths samples range from −17.9 to +15.7. However, direct comparisons of separate minerals and whole rock measurements for these samples provided strong evidence for diffusion-driven kinetic isotopic fractionation during the interactions of xenoliths with the host magma. Only the isotopically equilibrated xenoliths are likely to preserve the initial Li isotopic signature of the lower crust and were selected by Teng et al. (2008) as useful for this purpose. Based on these eight samples, the lower crust appears extremely heterogeneous, with δ^7Li ranging from -14‰ to +14.3‰ and a δ^7Li average of +1.6‰ ±8.9 (1σ) (Teng et al., 2008).

In order to constrain the Li isotopic characteristics of the lower continental crust as well as the HIMU mantle end-member, we studied a suite of volcanic rocks from Chaîne des Puys. This alkaline series was chosen because it is an archetype of a continental volcanic suite. It shows a complete petrologic range from basalts to trachytes (e.g., Maury et al., 1980), and geochemical variations within the series are remarkably coherent. Our goal is to model the geochemical evolution of the Chaîne des Puys series in order to constrain the mantle and crustal Li isotopic compositions of the involved reservoirs.

2. Geological setting and previous work.

The Chaîne des Puys is the youngest volcanic province of the French Massif Central (FMC), and the study of its well preserved volcanoes and lava flows has contributed to the development of volcanology in western Europe since the 18th century, following the pioneering work of Guettard (1752). It was emplaced between 100 ka and 8 ka over a deep N-S trending crustal fracture parallel to the nearby aborted Oligocene rift of the Limagne (Fig. 1). Most of its eruptive vents are clustered within a ca. 30 km long and 3 to 4 km wide volcanic axis, west of the town of Clermont-Ferrand.

104 The Chaîne des Puys lavas represent a typical mildly alkalic intraplate volcanic suite ranging from
105 alkali basalts and basanites to hawaiites, mugearites, and silica-oversaturated benmoreites and
106 trachytes. Alkali basalts, basanites and hawaiites form over a hundred strombolian cones up to 350 m
107 high with associated lava flows, as well as a dozen maars. Mugearites and benmoreites occur as ash
108 and scoria cones emitted as short and thick lava flows. The trachytes and a few benmoreites form four
109 domes (among which the eponymous Puy de Dôme), three protrusions, and several associated
110 pyroclastic flow deposits. The relative abundances of these petrological types roughly decrease from
111 basalts to mugearites and trachytes. Geochronological data (summarized in Boivin et al., 2004)
112 suggest that the emplacement of mafic magmas (basalts and hawaiites), which started around 100 ka,
113 was successively followed by that of mugearites and benmoreites (after 40 ka), and finally of trachytes
114 (mostly between 14 and 9 ka). Primitive mafic lavas are uncommon within the Massif, and most Mg-
115 rich compositions are those of basanitic melt inclusions trapped within olivine phenocrysts, which
116 might represent the parental magma of the suite (Jannot et al., 2005).
117
118 Petrographic and mineralogical data (summarized in Boivin et al., 2004) as well as major and trace
119 element data are consistent with a magmatic evolution mainly controlled by the fractional
120 crystallization of mafic melts, and involves separation of kaersutitic amphibole in intermediate
121 magmas (Maury et al., 1980; Villemant et al., 1980, 1981). In addition, the common occurrence of
122 partially melted continental crust xenoliths, together with the progressive increase of Sr and decrease
123 of Nd isotopic ratios from basalts to trachytes (Condomines et al., 1982; Chauvel and Jahn, 1984)
124 suggest the occurrence of crustal assimilation. The occurrence of deep-seated amphibole,
125 clinopyroxene, potassic oligoclase and scapolite megacrysts in mafic lavas (Boivin and Camus, 1981)
126 and of mixed trachybasaltic and trachytic pumices (Gourgaud and Camus, 1984) suggests that magmas
127 started their differentiation within deep reservoirs, probably located near the base of the French Massif
128 Central continental crust. Based on petrographical arguments, Boivin et al. (2004) proposed that
129 intermediate and residual liquids were generated within the continental crust.
130

Geophysical studies have shown that the Neogene and Quaternary volcanic activity in the FMC is associated with the upwelling of hot asthenospheric material (Lucazeau et al., 1984; Zeyen et al., 1997). This anomaly has been linked to a possible mantle plume located beneath the Massif Central (Granet et al., 1995, 2000; Sobolev et al., 1997). However, the lack of evidence for such a plume within the lower mantle has been interpreted as an indication of asthenospheric flow induced either by the delamination of the Alpine lithospheric root (Merle and Michon, 2001), or the retreat and sinking of the Apenninic slab (Barruol and Granet, 2002; Barruol et al., 2004).

Based on Sr, Nd, and Pb isotopic data on lavas, it has been proposed that the geochemical signature of the Neogene and Quaternary FMC volcanic provinces, including the Chaîne des Puys, is closely related to the HIMU reservoir. Indeed, it is characterized by low $^{87}Sr/^{86}Sr$ (< 0.7038) and high $^{206}Pb/^{204}Pb$ (> 19.5) ratios (Chauvel and Jahn, 1984; Downes, 1984; Wilson and Downes, 1991, 1992; Wilson et al., 1995). The origin of this geochemical signature is still a matter of debate (Downes, 2001; Wilson and Downes, 2006). Hoernle et al. (1995) have shown that it is shared by most Cenozoic volcanic provinces of Western and Central Europe, the Western Mediterranean domain, Northwestern Africa and the Canary islands. They have attributed its origin to the interactions between the European and Mediterranean lithospheric mantle and a large-scale asthenospheric plume linked to the opening of the Central Atlantic during the early Tertiary.

3. Samples and Analytical techniques

3.1. Samples.

Based on the detailed geochemical investigations undertaken by Villemant (1979) and Maury et al. (1980), 15 samples were selected (located in Fig. 1), which are representative of the entire Chaîne des Puys series. All samples were collected from fresh exposures of the Quaternary volcanics. Petrographic examinations reveal no evidences of secondary alteration, a conclusion that is supported by the low loss on ignition (LOI).

158 **3.2 Major and trace element analyses.**

159 Major element analyses were performed by ICP-AES at Centre de Recherches Pétrographiques et
160 Géochimiques, Nancy following the method described in Carignan et al. (2001). The precision of the
161 data, based on relative standard deviations, is better than 2%. Trace element analyses were performed
162 by ICP-MS at Grenoble following the procedure described in Barrat et al. (1996). The results obtained
163 for internationals standards (JB2, BHVO1, WSE and IFG) are reported in Barrat et al. (2000). Based
164 on standard measurements and sample duplicates, trace element concentration reproducibility is
165 generally better than 5%.

166

167 **3.3. Sr, Nd and Pb analyses.**

168 *3.3.1. Sr measurements.*

169 Isotopic compositions of Sr were determined at Géosciences Rennes. For Sr, rock powders were
170 leached for 3 hours in hot (150°C) 6N HCl, and rinsed in deionized water prior to dissolution.
171 Conventional ion exchange techniques were used for the separation of Sr and isotope ratio
172 measurements were carried out by thermal ionization mass spectrometry using a Finnigan Mat 262
173 equipped with seven collectors in static mode. Compositions are normalized for instrumental mass
174 fractionation relative to $^{86}Sr/^{88}Sr = 0.1194$. $^{87}Sr/^{86}Sr$ of the NBS 987 Sr standard yielded 0.710213±22
175 (2σ, n=14) and the sample Sr isotopic compositions are reported relative to $^{87}Sr/^{86}Sr = 0.71024$.

176

177 *3.3.2. Nd measurements.*

178 Isotopic compositions of Nd were measured at Institut Universitaire Européen de la Mer, Brest,
179 using a Thermo Finnigan, Triton. The measurements were carried out in static mode. The Nd
180 purification was done according to the procedure described in Dosso et al. (1993). TRU.Spec
181 chromatographic resins from Eichrom were used to separate the REE fraction from the sample matrix.
182 The separation and elution of Nd and other REE were realized on Ln.Spec. resin. During the course of
183 the study, analyses of the La Jolla standard were performed and give an average of $^{143}Nd/^{144}Nd =$
184 0.511845±6 (n = 15). All Nd data are fractionation corrected to $^{146}Nd/^{144}Nd = 0.7219$ and normalized

to a value of $^{143}Nd/^{144}Nd$ = 0.511860 for the La Jolla standard. Nd blanks measured using this procedure were < 0.5ng.

3.3.3. High-resolution Pb analyses.

Powdered samples were leached with 6 M HCl at 140°C for an hour and then rinsed up to six times with ultrapure water prior to dissolution. Lead separation was then performed on an anionic exchange resin. Pb analyses were carried out in static mode at Ifremer (Centre de Brest) on a Finnigan MAT 261 multi collector instrument upgraded by Spectromat, using the double spike technique with the calibrated Southampton-Brest 207/204 spike (Ishizuka et al., 2003). Replicate analyses of the Pb isotope standard NBS981 gave an average of 16.9432 ±0.0027 and 15.5004 ±0.0029 and 36.7326 ±0.0086 for $^{206}Pb/^{204}Pb$, $^{207}Pb/^{204}Pb$ and $^{208}Pb/^{204}Pb$, respectively (2σ, n=7). Pb blanks measured using this procedure were < 100pg, and thus negligible relative to the amount of sample analyzed.

3.4. Li analyses.

3.4.1. Whole rock Li isotopic measurements.

Li isotope chemistry and measurements were carried out at the Institut für Geowissenschaften, FE: Mineralogie, J.W. Goethe Universität Frankfurt. Rock digestion and column chemistry were completed following the procedure of Seitz et al. (2004). Powdered rock samples (15–25mg) were digested in a mixture of 1 ml 6 M HNO_3 and 1 ml concentrated HF. Subsequently, samples were dissolved in 6 M HCl and reconstituted in 6 M HNO_3 followed by chromatographic Li purification (see Seitz et al., 2004 for more detail). For Li-chromatography clear sample solutions of 0.18ml 5 M HNO_3 and 0.72ml 100% methanol (analytical grade) were passed through single, small 1.4ml exchange columns filled to height of 6 cm with BioRad AG50W-X8 (200–400 mesh) resin. With the collection of 10 ml of the eluate, all Li is recovered. To ensure 100% recovery we randomly checked pre and after cuts; Li was never detected in these. Measurements were performed using a Multi Collector Inductively Coupled Plasma Mass Spectrometer (MC-ICPMS, Neptune ThermoFinnigan) at dry plasma conditions using a Cetac Aridus® nebuliser fitted with a PFA-spray chamber and an ESI microconcentric-nebuliser. The analytical blank (chemistry blank and background signal on double

distilled 2% HNO_3) was usually 30-20 pg, ~12-20 mV on ^7Li. Sample analysis is carried out sequentially by 'bracketing' the sample with the L-SVEC standard (Flesch et al., 1973). Isotope compositions are expressed as per mil deviations from the NIST L-SVEC standard: (δ^7Li = $1000\times((^7Li/^6Li)_{sample} / (^7Li/^6Li)_{LSVEC} -1)$). Internal precision is typically between 0.2–0.6‰ (2σ). The best measure for the external precision is the long term reproducibility, determined by replicate dissolutions of the geological basalt standard JB-2 (δ^7Li of +5.1‰), which is about 1.2‰ (2σ).

3.4.2. In situ Li isotopic measurements.

In situ Li isotopic compositions were measured in olivine from sample Puy21 by the small radius (Cameca ims 3f) ion microprobe at Centre de Recherches Pétrographiques et Géochimiques (CRPG-CNRS, Nancy), using the analytical procedure previously described (Chaussidon and Robert, 1998; Beck et al., 2004, 2006; Barrat et al., 2005). Gold-coated polished samples were sputtered with an O- beam of approximately 25 μm size. The secondary $^6Li^+$ and $^7Li^+$ ions were accelerated at 4.5 kV and were counted in mono-collection mode with an electron multiplier using magnetic peak switching. The background on the two multipliers was monitored during the different sessions: it was below 0.05 cps (count per second). Recently, Bell et al. (2009) have shown a significant effect of the olivine composition on the Li isotope ratio measured by SIMS. This matrix effect is related to the Mg# of the olivine. In order to calibrate the instrumental mass fractionation for Li, it is important to select a standard with a forsterite component comparable to our sample. In our case, our sample presents a %Fo = 86.8 and the olivine standard (Olivine BZ29), presents a %Fo = 88.8. The instrumental mass fractionation ($\alpha_{inst}Li = (^7Li/^6Li)_{measured} / (^7Li/^6Li)_{true}$) ranged from ~1.020 to ~1.035 for our standard. Duplicate measurements made at different times in the same spot gave an estimate of reproducibility better than 2.5‰ (2σ).

4. Results

4.1. Major and trace elements variations

All samples have a very low loss of ignition (L.O.I. < 1.5%) reflecting the lack of alteration and the

240 pristine nature of the samples. Among the most primitive samples (with high Fe content), several show
241 negative L.O.I. results. This indicates that the weight increases arising from oxidation of Fe^{2+} to Fe^{3+}
242 (FeO to Fe_2O_3) is greater than the weight loss caused by removing volatiles from the mineral
243 structures. New data from this study are shown along with published analyses in the total alkali-SiO_2
244 diagram (Fig. 2). Our samples define a continuous suite, ranging from basalts (Na_2O+K_2O= 5.6wt%;
245 SiO_2 = 46.0wt%) with a MgO of 6.9wt% to trachytes (Na_2O+K_2O= 11.1wt%; SiO_2= 64.9wt%) with a
246 MgO of 0.5 wt%. This suite shows major element characteristics that are typical of mildly alkaline
247 rocks: high contents of Na_2O (from 3.3 to 6.6wt%) and K_2O (from 1.7 to 4.9wt%) increasing with
248 SiO_2 while total iron (as Fe_2O_3), MgO and CaO decrease (Maury et al., 1980; Boivin et al., 2004).
249
250 Corresponding trace element characteristics are also typical of mildly alkaline basaltic suites, with
251 high concentrations of incompatible elements such as Rb, Ba and Th (more than 150 times
252 concentration in the primitive mantle – Table 1). Chondrite-normalized Rare Earth Elements (REE)
253 show highly fractionated REE patterns $(La/Yb)_N$ > 13, along with significant changes in the trace
254 element patterns as a consequence of differentiation. The light REE enrichment increases from basalts
255 to trachytes, as evidenced by the variation of $(La/Sm)_N$ = 3.8 to 7.2. In contrast, over the same suite the
256 slopes of the heavy REE decrease from $(Gd/Yb)_N$ = 2.8 to 1.4. Therefore, intermediate and evolved
257 lavas display a progressively more concave REE pattern, which is linked to a medium REE depletion
258 attributed to amphibole fractionation (Villemant et al., 1980, 1981). Binary plots of trace elements vs
259 Th (see supplementary materials and Fig. 5) reveal three distinct stages, which correspond to
260 successive fractional crystallization during the magmatic evolution of the Chaîne des Puys melts.
261 These differentiation steps have been previously discussed in detail (e.g., Maury et al., 1980;
262 Villemant et al., 1980, 1981) and for our purpose only their major characteristics are recalled here. The
263 first two stages are linked to abundant crystallization of plagioclase and clinopyroxene. They differ
264 from each other by the disappearance of olivine and appearance of hornblende, apatite and Fe-Ti
265 oxides in the second stage. During the last differentiation step, the mineral assemblage changed
266 significantly with the crystallization of a great abundance of biotite, alkali feldspar, apatite and Fe-Ti
267 oxide.

4.2. Sr, Nd, Pb and Li isotopes

The Sr, Nd, Pb and Li isotopic compositions of the Chaîne des Puys samples show significant variations (Table 2). These variations are strongly linked to progressive differentiation. Basaltic lavas have low $^{87}Sr/^{86}Sr$ (≈ 0.7037), high $^{206}Pb/^{204}Pb$ (≈ 19.6), high ε_{Nd} (≈ 3.9) and heavy $\delta^{7}Li$ (≈ +7 ‰) signatures, whereas the evolved volcanic rocks display higher $^{87}Sr/^{86}Sr$ (≈ 0.7043), lower $^{206}Pb/^{204}Pb$ (≈ 19.3), lower ε_{Nd} (≈ 2.5) and lighter $\delta^{7}Li$ (≈ 0‰).

5. Discussion

5.1. AFC modeling based on Sr-Nd-Pb isotopes

Based on major and trace element data, it was suggested that the Chaîne des Puys alkalic basaltic suite is the result of fractional crystallization processes (Maury et al., 1980; Villemant et al. 1980, 1981). However, strong variations in radiogenic isotope compositions within the cogenetic alkalic series rule out a model of closed magmatic system evolution (Fig. 3) (Condomines et al., 1982; Downes, 1984; Wilson et al., 1995). When taking together the incompatible trace element ratios and the Sr, Nd, Pb, Li isotopic data, the chemical variations shown in Fig. 5 can be explained by the involvement of two distinct reservoirs:

(i) The first component is expressed in the least evolved volcanic rocks and is characterized by an HIMU-like isotopic signature (Wilson and Downes, 1991, 1992) with high Pb isotopic ratio ($^{206}Pb/^{204}Pb \approx 19.6$) and low $^{87}Sr/^{86}Sr$ ratio (< 0.7037).

(ii) The second component displays a slightly more radiogenic Sr isotopic compositions ($^{87}Sr/^{86}Sr > 0.7043$), lower ε_{Nd} and lower Pb isotopic ratios ($^{206}Pb/^{204}Pb < 19.3$), features that indicate unambiguously a continental crust component.

294 Clearly, the coherent variations of Sr, Nd and Pb isotopic compositions with the concentration of
295 an incompatible trace element, such as Th (or any differentiation index, e.g FeO/MgO) indicate the
296 assimilation of crustal rocks coupled with fractional crystallization (AFC: DePaolo, 1981). This
297 interpretation is strongly supported by field and petrographic observations (e.g., Maury and Bizouard,
298 1974) as well as radioactive disequilibrium data (Condomines et al., 1982). Our goal is to
299 quantitatively model the range in concentrations and variations in isotope compositions for Sr, Nd, Pb
300 and Li, using an AFC process (equations 6a and 15b from DePaolo, 1981). All parameters of the
301 model are presented in Table 3.
302
303 The first step in the AFC modeling is to identify the components involved in the process. In our
304 data set, none of the basalts is sufficiently primitive to be the direct result of mantle melting.
305 Therefore, we have selected the average of samples Puy21 and Puy16 to represent the initial liquid (l_o)
306 in our modeling. These samples are the most primitive samples studied here given their MgO and
307 compatible trace element contents (Mg# > 50 and Ni > 75 µg/g, Table 1). Constraining the
308 composition of the crustal contaminant involved in the AFC process is generally quite difficult. The
309 continental crust beneath the Chaîne des Puys volcanoes is very heterogeneous due to its complex
310 evolution during the Variscan orogeny. In this particular context, a possible contaminant is the upper
311 continental crust, which is mainly composed of Variscan granitoïds. However, their Pb isotopic ratios
312 are too low to represent the crustal component involved in the AFC process, as illustrated in Fig. 4.
313 Another possible contaminant is the lower crust. The nature of the FMC lower crust and lithospheric
314 mantle is mostly known from the study of xenoliths brought to the surface by Cenozoic alkaline
315 volcanic activity (Leyreloup et al., 1977; Downes and Dupuy, 1987; Downes, 1993). Three main types
316 of xenoliths have been identified: (i) mantle-derived ultramafic xenoliths (ii) meta-igneous granulites
317 and (iii) meta-sedimentary granulites. In order to find the most likely crustal contaminant, the
318 available analyses of all these types of lithologies are shown together with those of volcanic samples
319 of the Chaîne des Puys (Fig. 4). Based on Pb isotopes, which provide the best constraints on crustal
320 contamination, it appears that the meta-sedimentary granulites represent the main contaminant. In the
321 following section, the average composition of the meta-sedimentary granulites has been used in the

calculations (Downes et al., 1990; 1991). In contrast to the two-stage fractionation/assimilation process suggested by Boivin et al. (2004), all geochemical variations of the Chaîne des Puys samples presented here (Table 2 and supplementary materials) are satisfactorily explained by a single lower crustal contaminant.

Several parameters must be assumed in order to model the evolution of the volcanic series by the AFC process (DePaolo, 1981). Bulk distribution coefficients for each element (D_{Sr}, D_{Nd}, D_{Pb}, D_{Li}) have been evaluated using log C_a vs log C_b diagrams (a and b are two different trace elements). In these diagrams, if one element is highly incompatible (for example $D_b \approx 0$), the bulk distribution coefficient of the other element is directly estimated by the slope of the linear trend formed by the data (slope = 1-D_a). This method is adapted for fractionation in a closed magmatic system but is at first glance not suitable for AFC process because concentrations of trace elements do not directly depend on the fraction of residual liquid in the reservoir (F). Nevertheless, there is not much difference if D is calculated from a perfect Rayleigh fractionation process, except when AFC curves show marked inflection (Defant and Nielsen, 1990). In two element plots (Fig. 5 and supplementary materials), three distinct stages of the bulk distribution coefficients are noticeable, each one is associated with changes in the modal composition of cumulates. Calculated values of D_{Sr}, D_{Nd}, and D_{Pb}, for these steps are presented in Table 3. We assumed an initial $D_{Th} \approx 0$, changing to $D_{Th} = 0.2$ in order to account late stage crystallization of zircon.

Another important parameter in the AFC modeling is the ratio between the assimilation and the crystallization mass (r). There is no simple way to evaluate the absolute value of this ratio. For calculation purpose, however, we have initially considered a range for r from 0 (perfect fractional crystallization) to 0.3. The best fit is obtained for all three isotope systems for $r \approx 0.10$. As a first approximation in our model, this parameter is taken to be constant during the crystallization. The fact that the results are coherent for all three isotope systems indicates that the evolution of the Chaîne des Puys volcanics is the result of AFC processes that most likely occurred in lower crustal magma chambers. From basalts and hawaiites to trachytes, nearly 70% of the initial volume of liquid has

crystallized (Fig. 5). Similar results have been reported for other Quaternary alkaline series in the FMC (Wilson et al., 1995).

5.2 High δ^7Li in basaltic samples: a characteristic of the HIMU mantle end-member.

Because the least evolved lavas of the Chaîne des Puys are expected to have been least affected by crustal contamination effects, basaltic samples (Puy16, Puy21) are likely to resemble the isotopic composition of their mantle reservoirs. Based on Sr, Nd, and Pb radiogenic isotopic data, Wilson and Downes (1991) proposed that the FMC Cenozoic basaltic lavas have HIMU affinities (low $^{87}Sr/^{86}Sr$ (< 0.7038) and high $^{206}Pb/^{204}Pb$ (> 19.5)). However, the origin of this geochemical signature is still a matter of debate. The Li isotopic compositions (up to δ^7Li = +7‰) in FMC basalts are relatively heavy, compared to average fresh N-MORB ($\delta^7Li \approx +3.4‰ \pm 1.4$, Tomascak et al., 2008) and also differ from those of enriched mantle reservoirs (EM1 and EM2, Nishio et al., 2005) (Fig.6). Such heavy δ^7Li compositions have previously been reported in basaltic samples derived from HIMU mantle environment: lavas from the Austral Islands (Nishio et al., 2005; Chan et al., 2009) as well as from St Helena (Ryan and Kyle, 2004) and from peridotite xenoliths from the East African Rift (Aulbach et al., 2008). All these studies suggest that the heavy Li isotopes signature might reflect a typical feature of HIMU lavas.

Recently, Chan et al. (2009) reported a discrepancy between Li isotope data for whole rocks and mineral separates from Cook-Austral HIMU samples. These authors argued that the narrower range of δ^7Li values in olivine phenocrysts compared to the lavas is due to their lower susceptibility to post-magmatic alteration. Their work suggests that the heavy Li isotopes composition in HIMU basalts could be partially an artifact of sample alteration. Although our samples are much younger (< 100ka) than the samples used by Chan et al. (2009) (~ 20Ma), it is important to consider the potential effect of weathering. In order to compare whole rock and in situ Li measurements, an isotopic profile was measured on a single chemically homogeneous olivine phenocryst from the alkali basalt Puy21 (Fig. 7). Excluding extreme light δ^7Li values found near the crystal boundary and likely related to diffusion-induced Li isotopic fractionation (e.g., Barrat et al., 2005; Beck et al., 2006; Halama et al., 2007,

Hamelin et al., 2007), this phenocryst displays a homogeneous Li isotopic composition of +7.2‰. Assuming an analytical error (2σ) of ±2.5‰ for in situ data and ±1.2‰ for whole rock data, this value is indistinguishable from the whole rock analysis of this sample (δ^7Li = +6.7‰). Therefore, the Li isotopic composition of this crystal is in equilibrium with the melt. Our in situ data support the assumption that the heavy δ^7Li in the most primitive lavas from the Chaîne des Puys are genuine. In agreement with the final statement of Chan et al. (2009), our results suggest that the HIMU mantle is characterized by a significant enrichment in ^{7}Li.

Because the origin of the HIMU mantle is commonly assumed to be derived from recycled oceanic crust (Hofman and White, 1982), the hypothesis for the generation of the heavy Li-isotope signature has been influenced by the observation of a dramatically low δ^7Li value in eclogites (Zack et al., 2003). Jeffcoate and Elliott (2003) proposed that the source of HIMU magmas is initiated not from the dehydrated slab, but in the overlying mantle wedge. In their model, the heavy signature is produced by high δ^7Li fluids, which are released from the slab to the mantle wedge during dehydration. However, because fluids are enriched in Pb comparatively to U, this model fails to explain the high U/Pb ratio required to produce the high ^{206}Pb/^{204}Pb ratio in HIMU basalts. Nishio et al. (2005) proposed that, in contrast to the upper part of the oceanic crust, the moderately altered portion of the crust is preserved from the dehydration-induced Li isotopic fractionation during the subduction process and is therefore a potential source of the high δ^7Li HIMU signature. Based on experimental determination of mineral/fluid Li isotopic fractionation factors (Wunder et al., 2006; 2007), Marschall et al. (2007) called into question the assumption that altered oceanic crust will produce a light eclogitic residue during dehydratation and deep subduction. These authors argued that a great portion of Li could be retained in a deeply subducted slab. According to their model, the high δ^7Li produced by low-temperature alteration is not totally erased by subduction zone dehydration and therefore can be a source of HIMU geochemical signature. This hypothesis has been reexamined by Halama et al. (2008) by modeling Li diffusion at mantle temperatures. Their calculations predict that Li homogenization in the mantle is sufficiently effective to attenuate and erase heterogeneities over the time that is required to create the HIMU Pb isotopic signature. However, our results, which are in agreement with Chan et

406 al. (2009), suggest that the heavy Li isotopic signature of the altered oceanic crust is partially
407 preserved during subduction and is not completely erased by diffusion processes in the mantle.
408
409 **5.3. Application of the AFC model to the Li isotopes of the lower continental crust.**
410 Samples from the Chaîne des Puys volcanic suite show a very good correlation between Li
411 concentration and Li isotope composition (Fig. 8), ranging from low Li concentration (5.5 µg/g) and
412 relatively heavy isotopic compositions ($\delta^7Li \approx +7$ ‰) in basalts, to high concentrations (20 µg/g) and
413 lighter δ^7Li values ($\delta^7Li \approx +0.5$ ‰) in highly evolved melts. This trend is consistent with the
414 contamination of mantle-derived high δ^7Li melts with a low δ^7Li component. The Li content and
415 isotopic composition of the lower continental crust underlying the Quaternary volcanoes of the Chaîne
416 des Puys remains unknown. Because meta-sedimentary granulitic xenoliths are of a small size
417 (commonly less than 5 cm), their Li characteristics have potentially been corrupted by magma-
418 xenolith interdiffusion processes (e.g., Rudnick and Ionov, 2007; Ionov and Seitz, 2008). Recently,
419 direct comparison of δ^7Li in mineral separates and whole rock in granulite-facies xenoliths from China
420 and Australia have shown diffusion-driven kinetic isotopic fractionation during the interactions of
421 xenoliths with the host magma (Teng et al., 2008). The xenolith samples showing Li isotopic
422 equilibrium between mineral phases are likely to preserve the initial Li isotopic signatures of the lower
423 crust. Eight such granulite xenoliths measured by Teng et al. (2008) have δ^7Li value extending from -
424 14 ‰ to +14.3 ‰, with a concentration weighted average of +2.5 ‰ and a simple average of +1.6 ‰
425 ±8.9 (1σ). The lavas from the Chaîne des Puys provide a different approach to estimating the δ^7Li of
426 the lower crust. Our purpose is to use the AFC parameters determined with radiogenic isotopes in
427 order to constrain the Li characteristics of the contaminant component.
428
429 Solving the AFC equation for Li concentration and isotopic composition requires knowing (i) the
430 bulk solid/liquid distribution coefficient of Li during the fractional crystallization process (D_{Li}), (ii) the
431 Li content of the crustal component ($[Li]_c$), and finally (iii) the isotopic composition of the crustal
432 component (δ^7Li_c). It is important to note that any assumption made for one of these parameters allows
433 the calculation of the other two parameters by fitting the evolution in the liquid of the Li

concentrations and isotopic compositions. In order to fit the data, we use an iterative least squares method. It consists of adjusting the parameters of the AFC model function (equations 6a and 15b from DePaolo, 1981) so as to minimize the error with the data. This error (traditionally named χ) is defined as the sum of squared residuals, which are the difference between the observed values and values given by the model. This calculation has been performed for D_{Li} ranging from the unrealistic case where Li is seen as a perfectly incompatible element ($D_{Li} = 0$) to a moderately incompatible behavior ($D_{Li} = 0.4$). This range covers the value commonly accepted for D_{Li} during low pressure crystallization, which is found to be closed to 0.2–0.3 (Ryan and Langmuir, 1987). We assume that the ratio between the assimilation and the crystallization mass (r) for Li is coherent with the results found for the 3 radiogenic isotopes systems ($r = 0.10$). Nevertheless, to illustrate the influence of this parameter on the calculated Li characteristics in the contaminant, we repeated our calculation for $r = 0.06$ and $r = 0.14$ (Fig. 9).

The Li isotopic composition and abundance of the calculated crustal contaminant are illustrated in Fig. 9. Each solution represents a best-fitting curve of the evolution of the Li abundance and isotopic composition in the Chaîne des Puys volcanic suite. All together, the candidate solutions define the solution space of our model. If Li is seen as a perfectly incompatible element, the calculated $[Li]_c$ is in accordance with the previously estimated value in the lower continental crust (5-14 µg/g see Teng et al., 2008 and references therein). In this particular instance, a dramatically low δ^7Li_c value (< -20 ‰) is needed to reproduce the Li isotopic variation observed within the magmatic suite (Fig. 8). A more realistic (i.e. less incompatible) behavior of Li during the fractional crystallization process requires a higher Li content in the contaminant and therefore a less drastically low δ^7Li_c value. Ryan and Langmuir (1987) have shown that during low pressure crystallization, D_{Li} is closed to 0.2–0.3 and is broadly independent of the proportions of mineral phases involved. Therefore, using $D_{Li} = 0.3$ as a reasonable value, it is necessary to assume that $[Li]_c = 40$ µg/g in order to account for the evolution of Li concentration and a δ^7Li_c value of -5‰ is needed to reproduce the Li isotopic variation observed within the magmatic suite (Fig. 8). Because of the significant change in the mineral assemblage, limited variations of the Li bulk distribution coefficient during the differentiation sequence are

462 possible. This hypothesis implies a combined evolution of D_{Li} with another AFC parameter (r or $[Li]_c$)
463 in order to explain the constant slope on the plot of Li vs Th (Fig. 8). Therefore, a realistic model in
464 our solution space is defined by a trajectory along the differentiation sequence rather than a single
465 point.
466
467 **5.4 Low δ^7Li component: a lower continental crust characteristic or a consequence of kinetic**
468 **fractionation processes?**
469 The Li abundance required in our modeling is much higher than the average content in the lower
470 continental crust, ranging between 5 and 14 μg/g (Taylor and McLennan, 1985; Rudnick and Presper,
471 1990; Shaw et al., 1994; Rudnick and Fountain, 1995; Wedepohl, 1995; Gao et al. 1998). The high Li
472 concentration could be related to the sedimentary origin of the lower crustal parts beneath the Chaîne
473 des Puys, since shales have relatively high Li (25-110 ppm, Teng et al., 2004, Chan et al., 2006) and
474 metamorphic dehydration accounts for less than 50% loss (Teng et al., 2007). Concerning Li isotopes,
475 the low δ^7Li values calculated in the crustal component are within the range of δ^7Li measured in
476 equilibrated xenoliths (Teng et al., 2008). In the following sections, we discuss potential
477 interpretations to explain the Li composition of our calculated contaminant.
478
479 *5.4.1. Li isotopic composition of lower continental crust.*
480 Taking the assumption that the calculated contaminant is a direct estimation of the Li composition
481 of the meta-sedimentary part of the lower crust, it is interesting to address the question of the Li
482 isotopic composition of the protolith. Analysis of various types of sedimentary rocks from different
483 continents leads to a range of δ^7Li from -3.4 to +4.8‰ (Teng et al., 2004; Chan et al., 2006). The low
484 δ^7Li values calculated for the crustal component inferred from our AFC modeling are significantly
485 lower than any data from sedimentary rocks published so far (Teng et al., 2004). It seems therefore
486 unlikely that the low δ^7Li values are simply inherited from their protolith.
487
488 High-grade metamorphic rocks from the lower continental crust have undergone a complex thermal
489 and fluid history. Among the multitude of processes that may have affected their Li concentrations and

490 isotopic compositions, the first to be considered is progressive metamorphism during burial. Although
491 a majority of major and trace element contents in meta-sedimentary xenoliths are consistent with those
492 in greywacke-pelitic rocks, high grade metamorphism has significantly modified their large ion
493 lithophile element concentrations (e.g., Rb, Sr, Li) (Leyreloup et al., 1977). These xenoliths display
494 mineralogical characteristics that are typical for almost anhydrous granulite facies rocks (Downes and
495 Leyreloup, 1986). Therefore, it is likely that meta-sediments have released significant amounts of
496 water during their metamorphic evolution towards the granulite facies. Numerous studies have
497 demonstrated the high mobility of Li during fluid/rock interactions (e.g., Seyfried et al., 1998; Brenan
498 et al., 1998; Huh et al., 2001), and the elemental partitioning of Li between mineral and hydrous-fluids
499 ($D^{Min/Fluid}$) has been investigated experimentally under a variety of physical conditions (Berger et al.,
500 1988; Chan et al., 1994; Brenan al., 1998). During metamorphism, the Li partition coefficients
501 between crystals and aqueous fluid ($D^{Min/Fluid}$) drop from relatively high values for clays at low
502 temperature (0.35 for chlorites and 1.9 for smectites at 260°C, Berger et al., 1988), to very low values
503 for mineralogical assemblages under high grade metamorphic condition (0.16 for pyroxene and 0.008
504 for garnet at 900°C and 2 GPa, Brenan al., 1998). Because $D^{Min/Fluid}$ changes as a function of increasing
505 pressure and temperature, Li is released into the hydrous fluids during prograde metamorphic
506 evolution. Fractionation of Li isotopes during this dehydration process is explained by the preferential
507 affinity of the lighter isotope for the most highly coordinated site (Oi et al., 1989). Because Li often
508 substitutes for Mg, most silicate minerals contain eight-coordinated Li while in aqueous fluids, Li is
509 found in four-coordinate position (Wenger and Armbruster, 1991). Consequently, throughout the
510 dehydration process, equilibrium exchange between aqueous-fluids and Mg-silicates should lead to a
511 lower δ^7Li in the granulitic rocks. The amount of Li depletion and isotopic alteration depends of the
512 fractionation factor α ($[^7Li/^6Li]_{fluids}/[^7Li/^6Li]_{mineral}$) and the elemental partition coefficient $D^{Min/Fluid}$.
513 Recent experimental studies have shown that α is closely related to temperature, with greater isotope
514 fractionation during low temperature dehydration (Wunder et al., 2006, 2007). Therefore, the effects
515 of dehydration on Li isotopic fractionation are directly related to the evolution of temperature and
516 pressure conditions during prograde metamorphism. In agreement with this conclusion, negligible
517 effects of thermal metamorphism on δ^7Li were found for metapelites surrounding the Onawa granite

518 (Teng et al., 2007). The extent of δ^7Li modification during regional prograde metamorphism is less
519 clear, but is likely related to the amount of dehydration that takes place at low temperatures (Wunder
520 et al., 2006, 2007; Marschall et al., 2007). The role of this process to produce the light Li isotopic
521 signature in the lower crust is restricted by the limited isotopic fractionation occurring at temperatures
522 higher than 300°C (Wunder et al., 2006, 2007; Marschall et al., 2007).
523
524 *5.4.2. Isotopic fractionation during magmatic processes.*
525 Given the atypical Li characteristics of the contaminant involved in our modeling, we will examine
526 here whether this signature could be the result of isotopic fractionation either during fractional
527 crystallization or during anatexis of the assimilated crust.
528
529 The first potential process to be considered to explain the significant δ^7Li variations concomitant
530 with the progressive differentiation is that Li isotopes could be affected by mineral-melt fractionation.
531 Tomascak et al. (1999) were the first to address the question of mass-dependant equilibrium isotopic
532 fractionation process by studying samples from the Kilauea lava lake. The absence of per mil-level
533 variations of δ^7Li in their samples during olivine fractionation has shown the inefficiency of this
534 process at temperatures greater than 1050°C. More recently, direct comparison of olivine phenocrysts
535 and whole rock Li isotopes compositions in Hawaiian, Icelandic and Polynesian basalts have
536 confirmed the absence of isotopic fractionation (Chan and Frey, 2003; Jeffcoate et al., 2007; Chan et
537 al., 2009). The isotopic equilibrium seen between the olivine phenocryst and the whole rock in Puy 21
538 clearly supports this conclusion (Fig. 7). Because equilibrium isotope fractionation is temperature
539 dependant, this process could be more efficient during the last steps of the fractional crystallization.
540 However, in a recent study, Teng et al. (2009) have shown that δ^7Li does not correlate with any index
541 of granite differentiation, suggesting that Li isotope fractionation during crystallization is insignificant.
542 Given that Li is moderately incompatible in most mineral phases along a magmatic suite, it seems
543 unlikely that the large variations observed in our samples could be the result of equilibrium isotopic
544 fractionation between melt and minerals.
545

Another process capable of modifying Li isotopes is kinetic fractionation due to mass transport processes during melting of the lower crust. At high temperatures, equilibrium isotopic fractionations become negligible. Physical kinetic fractionations, on the other hand, are independent of temperature and thus can occur during these particular conditions and be preserved as long as the samples cool relatively quickly. During the differentiation of basaltic magma within deep reservoirs, Li diffusion from host granulites rocks into the magma could fractionate ^{6}Li and ^{7}Li by several per mil. Due to the higher diffusivity of the lighter isotope, melting of lower crustal granulites concomitant with the differentiation could therefore lead to an enrichment of ^{6}Li in the more evolved lavas, precluding the need for an exceptionally light Li isotope composition in the calculated contaminant. Whether or not these kinetic fractionations are significant will depend upon the time and length scale of the anatexis, the diffusion mechanisms, and the initial Li abundance ratio between meta-sedimentary granulites and the magma. During the initial steps of the magmatic evolution, Li abundances in the liquids are relatively low and the ratio with the estimated concentration in the surrounding lower crust is favorable for diffusion of Li from the lower crust into the melt. Because of the incompatible behavior of Li, the abundance ratio decreases with continuous differentiation and the amount of the kinetic fractionation should largely decrease for the more evolved liquids. Since many parameters are yet unknown, it is impossible to estimate unambiguously the extent of Li isotope fractionation that occurs during this process. Nevertheless, physical kinetic fractionation during the assimilation of lower crust is clearly an alternative process to explain the range of $\delta^{7}Li$ values determined for the Chaîne des Puys volcanic suite.

6. Conclusion

The intraplate volcanic series of the Chaîne des Puys shows large variations of Sr, Nd, Pb and Li isotopic ratios associated with progressive differentiation. These data suggest a magmatic evolution related to assimilation processes that occurred within magma chambers located in the lower crust. Using Sr, Nd and Pb isotopic composition of granulitic xenoliths, we have calculated input parameters

572 for the AFC modeling. We applied these parameters to characterize Li compositions of various
573 reservoirs involved in the AFC process:
574
575 (i) The mantle end-member: Expressed in the least evolved lavas, the isotopic composition of the
576 mantle component has clearly an HIMU affinity. The Li isotope composition of this reservoir has a
577 relatively heavy signature ($\delta^7Li \geq +7‰$). This result is in good agreement with previous δ^7Li
578 measurements of OIB lavas with HIMU affinities (Ryan and Kyle, 2004; Nishio et al., 2005; Chan et
579 al., 2009) (Fig. 7). Along with our observations, these results suggest that heavy Li isotope
580 compositions of altered oceanic crust can be reintroduced and partially preserved in deeper mantle
581 regimes.
582
583 (ii) The lower crust end-member: Mixing relationships throughout the AFC process along the
584 Chaîne des Puys volcanic suite allow us to place constraints on the Li signature of the lower crustal
585 end-member. Hence, this calculation gives an indirect method to assess the in situ value of δ^7Li in a
586 portion of the lower crust beneath the FMC. Using $D_{Li} = 0.3$ as a reasonable value, it is necessary to
587 assume that $[Li]_c = 40\mu g/g$ in order to account for the evolution of Li concentration within the
588 magmatic suite. In this particular case a δ^7Li_c value of -5‰ is needed to reproduce the Li isotopic
589 variation observed within the magmatic suite (Fig. 9). The Li abundance of the calculated contaminant
590 is higher than previous estimations of the lower continental crust (5 to 14µg/g, Teng et al., 2008 and
591 references therein), but consistent with a metapelitic contaminant. The low δ^7Li signature in the
592 calculated contaminant falls in the range defined by equilibrated lower crustal xenoliths (Teng et al.,
593 2008). However, it is important to note that the behavior of Li isotopes during assimilation process is
594 not yet known and that alternative interpretations cannot entirely be ruled out.
595
596
597
598
599

Acknowledgments

We gratefully acknowledge the Programme Dyeti (CNRS-INSU) for financial support. We thank R. Rudnick for the editorial handling and two anonymous reviewers for constructive comments. Li isotopes in situ data would not have been obtained without the assistance of Denis Mangin, Michel Champenois and Claire Rollion-Bard during the SIMS analyses. We acknowledge Marion Thomas, Claire Waller and Kristin Bergmann for their valuable comments and Marcel Bohn for his help with the electron microprobe. The hospitality of Francis Barrat and his family during the sampling expedition has been highly appreciated.

References

Aulbach, S., Rudnick, R. L., and McDonough, W. F., 2008. Li-Sr-Nd isotope signatures of the plume and cratonic lithospheric mantle beneath the margin of the rifted Tanzanian craton (Labait). *Contrib. Mineral. Petrol. 155*, 79–92.

Barrat, J.-A., Keller, F., Amosse, J., Taylor, R. N., Nesbitt, R. W., and Hirata, T., 1996. Determination of rare earth elements in sixteen silicate reference samples by ICP-MS using a Tm addition and an ion exchange chromatography procedure. *Geostandards Newsletter 20*, 133–139.

Barrat, J.-A., Blichert-Toft, J., Gillet, Ph., and Keller, F., 2000. The differentiation of eucrites: The role of in-situ crystallization. *Meteorit. Planet. Sci. 35*, 1087–1100.

Barrat, J.-A., Chaussidon, M., Bohn, M., Gillet, P., Gopel, C., and Lesourd, M., 2005. Lithium behavior during cooling of a dry basalt: An ion-microprobe study of the lunar meteorite Northwest Africa 479 (NWA 479). *Geochim. Cosmochim. Acta 69*, 5597–5609.

Beck, P., Barrat, J.-A., Chaussidon, M., Gillet, P., and Bohn, M., 2004. Li isotopic variations in single pyroxenes from the Northwest Africa 480 shergottite (NWA 480): a record of degassing of Martian magmas? *Geochim. Cosmochim. Acta 68*, 2925–2933.

Beck, P. Chaussidon, M., Barrat, J.-A., Gillet, P., and Bohn, M., 2006. Diffusion induced Li isotopic fractionation during the cooling of magmatic rocks: The case of pyroxene phenocrysts from nakhlite meteorites. *Geochim. Cosmochim. Acta 70*, 4813–4825.

Bell, D.R., Hervig, R.L., Buseck, P.R. and Aulbach, S., 2009. Lithium isotope analysis of olivine by SIMS: Calibration of a matrix effect and application to magmatic phenocrysts. *Chem. Geol.*, *258*, 5-16.

Barruol, G., Deschamps, A. and Coutant, O., 2004. Mapping upper mantle anisotropy beneath SE France by SKS splitting indicates Neogene asthenospheric flow induced by Apenninic slab roll-back and deflected by the deep Alpine roots. *Tectonophysics 394*, 125–138.

Barruol, G. and Granet, M., 2002. A Tertiary asthenospheric flow beneath the southern French Massif Central indicated by upper mantle seismic anisotropy and related to the west Mediterranean extension. *Earth Planet. Sci. Lett. 202*, 31–47.

Berger, G., Schott, J., and Guy, C., 1988. Behavior of Li, Rb and Cs during basalt glass and olivine dissolution and chlorite, smectite and zeolite precipitation from seawater – Experimental investigations and modelization between 50°C and 300°C, *Chem. Geol. 71*, 297–312.

Boivin, P., Besson, J.-L., Briot, D., Gourgaud, A., Labazuy, P., de Larouzière, F.D., Livet, M., Mergoil, J., Miallier, D., Morel, J.-M., Vernet, G. and Vincent, P., 2004. Volcanologie de la Chaîne des Puys, 4ème édition. Parc Naturel Régional des Volcans d'Auvergne, Aydat, 179 p.

Boivin, P. and Camus, G., 1981. Igneous scapolite-bearing associations in the Chaîne des Puys, Massif Central (France) and Atakor, Hoggar (Algeria). *Contrib. Mineral. Petrol. 77*, 365–375.

Brenan, J. M., Ryerson, F. J., and Shaw, H. F., 1998. The role of aqueous fluids in the slab-to-mantle transfer of boron, beryllium and lithium during subduction: Experiments and models, *Geochim. Cosmochim. Acta 62*, 3337–3347.

Carignan, J., Hild, P., Mevelle, G., Morel, J., and Yeghicheyan, D., 2001. Routine Analyses of Trace Elements in Geological Samples using Flow Injection and Low Pressure On-Line Liquid Chromatography Coupled to ICP-MS: A Study of Geochemical Reference Materials BR, DR-N, UB-N, AN-G and GH. *Geostandards Newsletter 25*, 187–198.

655 Chan, L.-H., Edmond, J.-M., Thompson, G., and Gillis, K., 1992. Lithium isotopic composition of
656 submarine basalts: implications for the lithium cycle in the oceans. *Earth Planet. Sci. Lett. 108*,
657 151–160.
658 Chan, L.-H., Gieskes, J.-M. Chen-Feng, Y. and Edmond, J.-M., 1994. Lithium isotope geochemistry
659 of sediments and hydrothermal fluids of the Guaymas Basin, Gulf of California. *Geochim.*
660 *Cosmochim. Acta 58*, 4443–4454.
661 Chan, L.-H. and Frey, F. A., 2003. Lithium isotope geochemistru of the Hawaiian plume: Results from
662 the Hawaii Scientific Drilling Project and Koolau Volcano. *Geochem. Geophys. Geosyst. 4*.
663 Chan, L.-H., Leeman, W. P., Plank, T., 2006. Lithium isotopic composition of marine sediments,
664 *Geochem. Geophys. Geosyst. 7*, Q06005, doi:10.1029/2005GC001202.
665 Chan, L.-H., Lassiter, J. C., Hauri, E. H., Hart, S. R. and Blusztajn, J., 2009. Lithium isotope
666 systematics of lavas from the Cook-Austral Islands: Constraints on the origin of HIMU mantle.
667 *Earth Planet. Sci. Lett.277*, 433-442.
668 Chaussidon, M. and Robert, F., 1998. $^{7}Li/^{6}Li$ and $^{11}B/^{10}B$ variations in chondrules from the Semarkona
669 unequilibrated chondrite. *Earth Planet. Sci. Lett. 164*, 577-589.
670 Chauvel, C. and Jahn, B. M., 1984. Nd-Sr isotope and REE geochemistry of alkali basalts from the
671 Massif Central, France. *Geochim. Cosmochim. Acta 48*, 93-110.
672 Condomines, M., Morand, P., Camus, G., and Duthou, L., 1982. Chronological and geochemical study
673 of lavas from the Chaîne des Puys, Massif Central, France: evidence for crustal contamination.
674 *Contrib. Mineral. Petrol. 81*, 296–303.
675 Defant, M. J. and Nielsen, R. L., 1990. Interpretation of open system petrogenetic processes: Phase
676 equilibria constraints on magma evolution. *Geochim. Cosmochim. Acta 54*, 87–102.
677 DePaolo, D. J., 1981. Trace-element and isotopic effects of combined wallrock assimilation and
678 fractional crystallisation. *Earth Planet. Sci. Lett. 53*, 189–202.
679 Dosso, L., Bougault, H., Joron, J.L., 1993 Geochemical morphology of the North Mid-Atlantic Ridge,
680 10°–24°N: trace element–isotopes complementarity, *Earth Planet. Sci. Lett. 120,* 443–462.
681 Downes, H., 1984. Sr and Nd isotope geochemistry of coexisting alkaline series, Cantal, Massif
682 Central, France. *Earth Planet. Sci. Lett. 69*, 321–334.
683 Downes, H., 1993. The nature of the lower continental crust of Europe: petrological and geochemical
684 evidence from xenoliths. *Phys. Earth Planet. Int. 79*, 195–218.
685 Downes, H., 2001. Formation and modification of the shallow sub-continental lithospheric mantle: a
686 review of geochemical evidence from ultramafic xenolith suites and tectonically emplaced
687 ultramafic massifs of Western and Central Europe. *J. Petrol. 42*, 233–250.
688 Downes, H. and Dupuy, C., 1987. Textural, isotopic and REE variations in spinel peridotite xenoliths,
689 Massif Central, France. *Earth Planet. Sci. Lett. 82*, 121–135.
690 Downes, H. and Leyreloup, A., 1986. Granulitic xenoliths from the French Massif Central: petrology,
691 Sr and Nd isotope systematics and model age estimates. *Geol. Soc. London, Special Publ. 24*,
692 319–330.
693 Downes, H., Dupuy, C., and Leyreloup, A. F., 1990. Crustal evolution of the Hercynian belt of
694 Western Europe: Evidence from lower-crustal granulitic xenoliths (French Massif Central).
695 *Chem. Geol. 83*, 209–231.
696 Downes, H., Kempton, P. D., Briot, D., Harmon, R. S., and Leyreloup, A. F., 1991. Pb and O isotope
697 systematics in granulite facies xenoliths, French Massif Central: implications for crustal
698 processes. *Earth Planet. Sci. Lett. 102*, 342–357.
699 Downes, H., Shaw, A., Williamson, B.J., and Thirlwall, M.F., 1997. Hercynian granodiorites and
700 monzogranites, Massif Central, France. *Chem. Geol. 136*, 99–122.
701 Elliott, T., Thomas, A., Jeffcoate, A., and Niu, Y., 2006. Lithium isotope evidence for subduction-
702 enriched mantle in the source of mid-ocean-ridge basalts. *Nature 443*, 565–568.

703 Flesh, G. D., Anderson, A. R., and Svec, H. J., 1973. A secondary isotopic standard for 7Li/6Li
704 determination. *Int. J. Mass Spectrom. 12*, 265–272.
705 Foustoukos, D.I., James, R.H., Berndt, M.E., and Seyfried, J.W.E., 2004. Lithium isotopic systematics
706 of hydrothermal vent fluids at the Main Endeavour Field, Northern Juan de Fuca Ridge. *Chem.*
707 *Geol. 212*, 17–26.
708 Gao, S., Luo, T.-C., Zhang, B.-R., Zhang, H.-F., Han, Y.-W., Hu, Y.-K., and Zhao, Z.-D., 1998.
709 Chemical composition of the continental crust as revealed by studies in east China. *Geochim.*
710 *Cosmochim. Acta 62*, 1959–1975.
711 Granet, M., Wilson, M., and Achauer, U., 1995. Imaging a plume beneath the French Massif Central.
712 *Earth Planet. Sci. Lett. 136*, 281–296.
713 Granet, M., Judenherc, S. and Souriau, A., 2000. Des images du système lithosphère-asthénosphère
714 sous la France et leurs implications géodynamiques : l'apport de la tomographie télésismique et
715 de l'anisotropie sismique. *Bull. Soc. Geol. France 171*, 149–167.
716 Gourgaud, A. and Camus, G., 1984. Magma mixing at La Nugère (Chaîne des Puys, Massif Central,
717 France). Role in trachyandesite genesis. *Bull. Volcanol. 47(4)*, 781–805.
718 Guettard, J.-E., 1752. Mémoire sur quelques montagnes de la France qui ont été des volcans. *Mém.*
719 *Acad. Roy. Sci*., Paris, 27-59.
720 Halama, R., McDonough, W. F., Rudnick, R. L., Keller, J. and Klaudius, J., 2007. The Li isotopic
721 composition of Oldoinyo Lengai: Nature of the mantle sources and lack of isotopic fractionation
722 during carbonatite petrogenesis. *Earth Planet. Sci. Lett. 254*, 77-89.
723 Halama, R., McDonough, W. F., Rudnick, R. L., and Bell, K., 2008. Tracking the lithium isotopic
724 evolution of the mantle using carbonatites. *Earth Planet. Sci. Lett. 265*, 726–742.
725 Hamelin, C., Chaussidon, M., Barrat, J.-A., Beck, P. and Bohn, M., 2007. Li diffusion and isotopic
726 fractionation in olivines crystals. *Geochim. Cosmochim. Acta 71*, A373–A373.
727 Hoernle, K., Zhang, Y.-S., and Graham, D., 1995. Seismic and geochemical evidence for large-scale
728 mantle upwelling beneath the eastern Atlantic and western and central Europe. *Nature 374*, 34–
729 39.
730 Hofmann, A. W., and White, W. M., 1982. Mantle plumes from ancient oceanic crust. *Earth Planet.*
731 *Sci. Lett. 57*, 421–436.
732 Huh, Y., Chan, L.-H., Zhang, L., and Edmond, J. M., 1998. Lithium and its isotopes in major world
733 rivers: implications for weathering and the oceanic budget. *Geochim. Cosmochim. Acta 62*,
734 2039–2051.
735 Huh, Y., Chan, L.-H., and Edmond, J. M., 2001. Lithium isotopes as a probe of weathering processes:
736 Orinoco River. *Earth Planet. Sci. Lett. 194*, 189–199.
737 Ionov, D.A. and Seitz, H.-M., 2008. Lithium abundances and isotopic compositions in mantle
738 xenoliths from subduction and intra-plate settings: Mantle sources vs. eruption histories. *Earth*
739 *Planet. Sci. Lett. 266*, 77–89.
740 Ishizuka, O., Taylor, R. N., Milton, J. A., and Nesbitt, R. W., 2003. Fluid-mantle interaction in an
741 intra-oceanic arc: constraints from high-precision Pb isotopes. *Earth Planet. Sci. Lett. 211*, 221–
742 236.
743 Jannot, S., Schiano, P. and Boivin, P., 2005. Melt inclusions in scoria and associated mantle xenoliths
744 of Puy Beaunit Volcano, Chaîne des Puys, Massif Central, France. *Contrib. Mineral. Petrol.*
745 *149*, 600–612.
746 Jeffcoate, A., and Elliott, T., 2003. Tracing recycled Li in the mantle: insights into mantle
747 heterogeneities. *EOS Trans. AGU 84*, V52A-0416.
748 Jeffcoate, A. B., Elliott, T., Kasemann, S. A., Ionov, D., Cooper, K. and Brooker, R., 2007. Li isotope
749 fractionation in peridotites and mafic melts. *Geochim. Cosmochim. Acta 71*, 202-218.
750 Kisakurek, B., Widdowson, M., and James, R. H., 2004. Behaviour of Li isotopes during continental

751 weathering: the Bidar laterite profile, India. *Chem. Geol. 212*, 27–44.
752 Lentz, R.C.F., McSween, H.Y., Jr., Ryan, J., and Riciputi, L.R., 2001. Water in Martian magmas:
753 clues from light lithophile elements in shergottite and nakhlite pyroxenes. *Geochim.*
754 *Cosmochim. Acta 65*, 4551–4565.
755 Leyreloup, A., Dupuy, C. and Andriambololona, R., 1977. Catazonal xenoliths in French Neogene
756 volcanic rocks: constitution of the lower crust. *Contrib. Mineral. Petrol. 62*, 283–300.
757 Lucazeau, F., Vasseur, G. and Bayer, R., 1984. Interpretation of heat flow data in the french Massif
758 Central. *Tectonophysics 103*, 99–119.
759 Lundstrom, C. C., Chaussidon, M., Hsui, A. T., Kelemen, P., and Zimmerman, M., 2005. Observations
760 of Li isotopic variations in the Trinity Ophiolite: Evidence for isotopic fractionation by
761 diffusion during mantle melting. *Geochim. Cosmochim. Acta* 69, 735–751.
762 Marschall, H. R., Pogge von Strandmann, P. A. E., Seitz, H.-M., Elliott, T., and Niu, Y., 2007. The
763 lithium isotopic composition of orogenic eclogites and deep subducted slabs. *Earth Planet. Sci.*
764 *Lett. 262*, 563–580.
765 Maury, R.C. and Bizouard, H., 1974. Melting of acid xenoliths into a basanite: an approach to the
766 possible mechanisms of crustal contamination. *Contrib. Mineral. Petrol. 48*, 275–286.
767 Maury, R.C., Brousse, R., Villemant, B., Joron, J.-L., Jaffrezic, H. and Treuil, M., 1980. Cristallisation
768 fractionnée d'un magma basaltique alcalin: la série de la Chaîne des Puys (Massif Central,
769 France). I. Pétrologie. *Bulletin de Minéralogie 103*, 250–266.
770 Merle, O. and Michon, R., 2001. The formation of the West European Rift: a new model as
771 exemplified by the Massif Central area. *Bull. Soc. géol. France*, 172, 213–221.
772 Millot, R., Negrel, P., and Petelet-Giraud, E., 2007. Multi-isotopic (Li, B, Sr, Nd) approach for
773 geothermal reservoir characterization in the Limagne Basin (Massif Central, France). *Appl.*
774 *Geochem. 22*, 2307–2325.
775 Moriguti, T. and Nakamura, E., 1998. Across-arc variation of Li isotopes in lavas and implications for
776 crust/mantle recycling at subduction zones. *Earth Planet. Sci. Lett. 163*, 167-174.
777 Nishio, Y., Nakai, S. I., Kogiso, T., and Barsczus, H. G., 2005. Lithium, strontium, and neodymium
778 isotopic compositions of oceanic island basalts in the Polynesian region: constraints on a
779 Polynesian HIMU origin. *Geochem. J. 39*, 91–103.
780 Nishio, Y., Nakai, S. i., Ishii, T. and Sano, Y., (2007). Isotope systematics of Li, Sr, Nd, and volatiles
781 in Indian Ocean MORBs of the Rodrigues Triple Junction: Constraints on the origin of the
782 DUPAL anomaly. *Geochim. Cosmochim. Acta 71*, 745–759.
783 Oi, T., Nomura, M., Musashi, M., Ossaka, T., Okamoto, M., Kakihana, H., 1989. Boron isotopic
784 composition of some boron minerals, *Geochim. Cosmochim. Acta 53,* 3189–3195.
785 Ryan, J.G. and Langmuir, C.H., 1987. The systematics of lithium abundances in young volcanic rocks.
786 *Geochim. Cosmochim. Acta 51*, 1727–1741.
787 Ryan, J.G. and Kyle, P. R., 2004. Lithium abundance and lithium isotope variations in mantle sources:
788 insights from intraplate volcanic rocks from Ross Island and Marie Byrd Land (Antarctica) and
789 other oceanic islands. *Chem. Geol. 212*, 125–142.
790 Rudnick, R. L. and Presper, T., 1990. Geochemistry of intermediate to high-pressure granulites. In
791 Granulites and Crustal Evolution (eds. D. Vielzeuf and P. Vidal). Kluwer, Amsterdam, pp. 523–
792 550.
793 Rudnick, R. L. and Fountain, D. M. 1995. Nature and composition of the continental crust: a lower
794 crustal perspective. *Rev. Geophys. 33(3)*, 267–309.
795 Rudnick, R. L., Tomascak, P. B., Njo H. B., and Gardner, L. R., 2004. Extreme lithium isotopic
796 fractionation during continental weathering revealed in saprolites from South Carolina. *Chem.*
797 *Geol. 212*, 45–57.

798 Rudnick, R. L., and Ionov, D. A., 2007. Lithium elemental and isotopic disequilibrium in minerals
799 from peridotite xenoliths from far-east Russia: Product of recent melt/fluid-rock reaction. *Earth*
800 *Planet. Sci. Lett. 256,* 278-293.
801 Seitz, H.-M., Brey, G. P., Lahaye, Y., Durali, S., and Weyer, S., 2004. Lithium isotopic signatures of
802 peridotite xenoliths and isotopic fractionation at high temperature between olivine and
803 pyroxenes. *Chem. Geol. 212*, 163–177.
804 Seyfried, Jr. W.E., Chen, X., and Chan, L.-H., 1998. Trace element mobility and lithium isotope
805 exchange during hydrothermal alteration of seafloor weathered basalt: An experimental study at
806 350°C, 500 bars, *Geochim. Cosmochim. Acta 62*, 949–960.
807 Shaw, D. M., Dickin, A. P., Li, H., McNutt, R. H., Schwarcz, H. P., and Truscott, M. G., 1994. Crustal
808 geochemistry in the Wawa-Foleyet region, Ontario. *Can. J. Earth Sci. 31(7)*, 1104–1121.
809 Sobolev, S.V., Zeyen,, H., Granet M., Achauer, U., Werling, F., Altherr, R. and Fuchs, Y., 1997.
810 Upper mantle temperatures and lithosphere-asthenosphere system beneath the French Massif
811 Central constrained by seismic, gravity, petrologic and thermal observations. *Tectonophysics*
812 *275*, 143–164.
813 Taylor, S. R. and McLennan, S. M., 1985. The Continental Crust: Its Composition and Evolution.
814 Blackwell, Oxford.
815 Teng, F. Z., McDonough, W. F., Rudnick, R. L., Dalpe, C., Tomascak, P. B., Chappell, B. W., and
816 Gao, S., 2004. Lithium isotopic composition and concentration of the upper continental crust.
817 *Geochim. Cosmochim. Acta 68*, 4167–4178.
818 Teng, F.-Z., McDonough, W. F., Rudnick, R. L., and Walker, R. J., 2006. Diffusion-driven extreme
819 lithium isotopic fractionation in country rocks of the Tin Mountain pegmatite. *Earth Planet. Sci.*
820 *Lett. 243*, 701-710.
821 Teng, F.-Z., McDonough, W. F., Rudnick, R. L. and Wing, B. A., 2007. Limited lithium isotopic
822 fractionation during progressive metamorphic dehydration in metapelites: A case study from the
823 Onawa contact aureole, Maine. *Chem. Geol. 239*, 1-12.
824 Teng, F.-Z., Rudnick, R. L., McDonough, W. F., Gao, S., Tomascak, P. B. and Liu, Y., 2008. Lithium
825 isotopic composition and concentration of the deep continental crust. *Chem. Geol. 255*, 47-59.
826 Teng, F.-Z., Rudnick, R. L., McDonough, W. F. and Wu, F.-Y., Lithium isotopic systematics of A-
827 type granites and their mafic enclaves: Further constraints on the Li isotopic composition of the
828 continental crust. *Chem. Geol.,* In Press, Corrected Proof.
829 Tomascak, P. B., Tera, F., Helz, R. T., and Walker, R. J., 1999. The absence of lithium isotope
830 fractionation during basalt differentiation: new measurements by multicollector sector ICP-MS.
831 *Geochim. Cosmochim. Acta 63*, 907-910.
832 Tomascak, P. B., Langmuir, C. H., le Roux, P. J., and Shirey, S. B., 2008. Lithium isotopes in global
833 mid-ocean ridge basalts. *Geochim. Cosmochim. Acta 72*, 1626–1637.
834 Villemant, B., 1979. Etude géochimique des éléments en traces dans les séries volcaniques du Massif
835 Central. Thèse 3° cycle. Jussieu. 223p
836 Villemant, B., Joron, J.-L., Jaffrezic, H., Treuil, M., Maury, R.C. and Brousse, R., 1980. Cristallisation
837 fractionnée d'un magma basaltique alcalin: la série de la Chaîne des Puys (Massif Central,
838 France). II. Géochimie. *Bulletin de Minéralogie 103*, 267–286.
839 Villemant, B., Joron, J.-L., Jaffrezic, H. and Treuil, M., 1981. Distribution coefficients of major and
840 trace elements: fractional crystallization in the alkali basalt series of Chaîne des Puys (Massif
841 Central, France). *Geochim. Cosmochim. Acta 45*, 1997–2016.
842 Wagner, C. and Deloule, E., 2007. Behaviour of Li and its isotopes during metasomatism of French
843 Massif Central lherzolites. *Geochim. Cosmochim. Acta 71*, 4279–4296.
844 Wedepohl, H.,1995. The composition of the continental crust. *Geochim. Cosmochim. Acta 59*, 1217–
845 1239.

Wenger, M., and Armbruster, T., 1991. Crystal-chemistry of lithium oxygen coordination and bonding, *Eur. J. Mineral*. *3*, 387–399.

Wilson, M. and Downes, H., 1991. Tertiary-Quaternary Extension-Related Alkaline Magmatism in Western and Central Europe. *J. Petrol. 32*, 811–849.

Wilson, M. and Downes, H., 1992. Mafic alkaline magmatism associated with the European Cenozoic Rift system. *Tectonophysics 208*, 173–182.

Wilson, M., Downes, H., and Cebria, J.-M., 1995. Contrasting fractionation trends in coexisting continental alkaline magma series; Cantal, Massif Central, France. *J. Petrol. 36*, 1729–1753.

Wilson, M. and Downes, H., 2006. Tertiary-Quaternary intra-plate magmatism in Europe and its relationship to mantle dynamics. In: Gee D.G. and Stephenson R. (eds), European lithosphere dynamics. *Geol. Soc. London Memoir 32*, 167–190.

Wunder, B., Meixner, A., Romer, R.L., and Heinrich, W., 2006. Temperature-dependent isotopic fractionation of lithium between clinopyroxene and high-pressure fluids. *Contrib. Mineral. Petrol. 151*, 112–120.

Wunder, B., Meixner, A., Romer, R.L., Feenstra, A., Schettler, G., and Heinrich, W., 2007. Lithium isotope fractionation between Li-bearing staurolite, Li-mica and aqueous fluids: An experimental study. *Chem. Geol. 238*, 277–290.

Zack, T., Tomascak, P. B., Rudnick, R. L., Dalpe, C., and McDonough, W. F., 2003. Extremely light Li in orogenic eclogites: The role of isotope fractionation during dehydration in subducted oceanic crust. *Earth Planet. Sci. Lett. 208*, 279–290.

Zeyen, H., Novak, O., Landes, M., Prodhel, C., Driad, L. and Hirn, A., 1997. Refraction-sismic investigations of the northern Massif Central (France). *Tectonophysics 275*, 99–117.

Figure 1

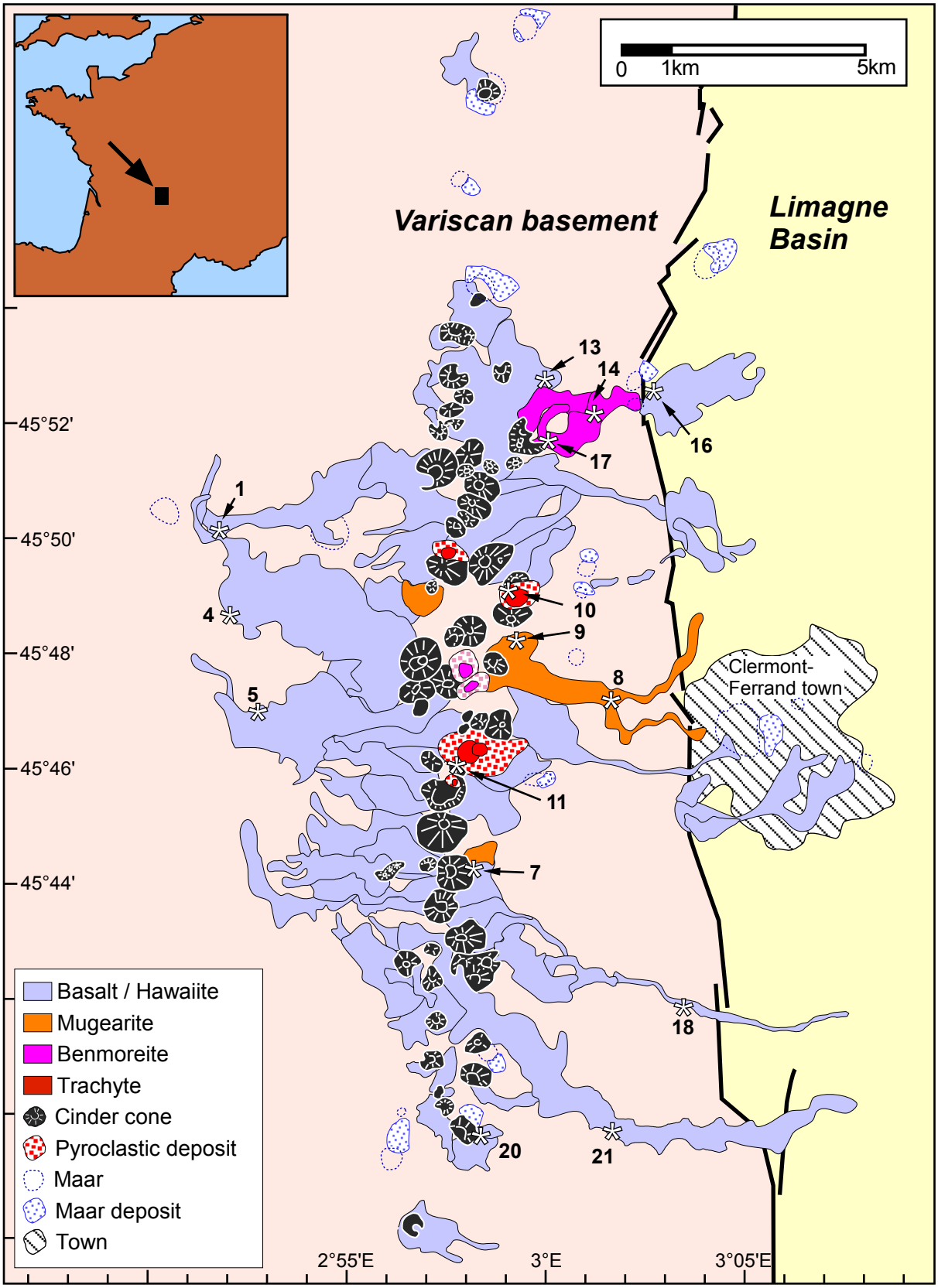

Figure 1: Simplified geological map showing major features of the Chaîne des Puys volcanic activity, as well as sample numbers.

Figure 2

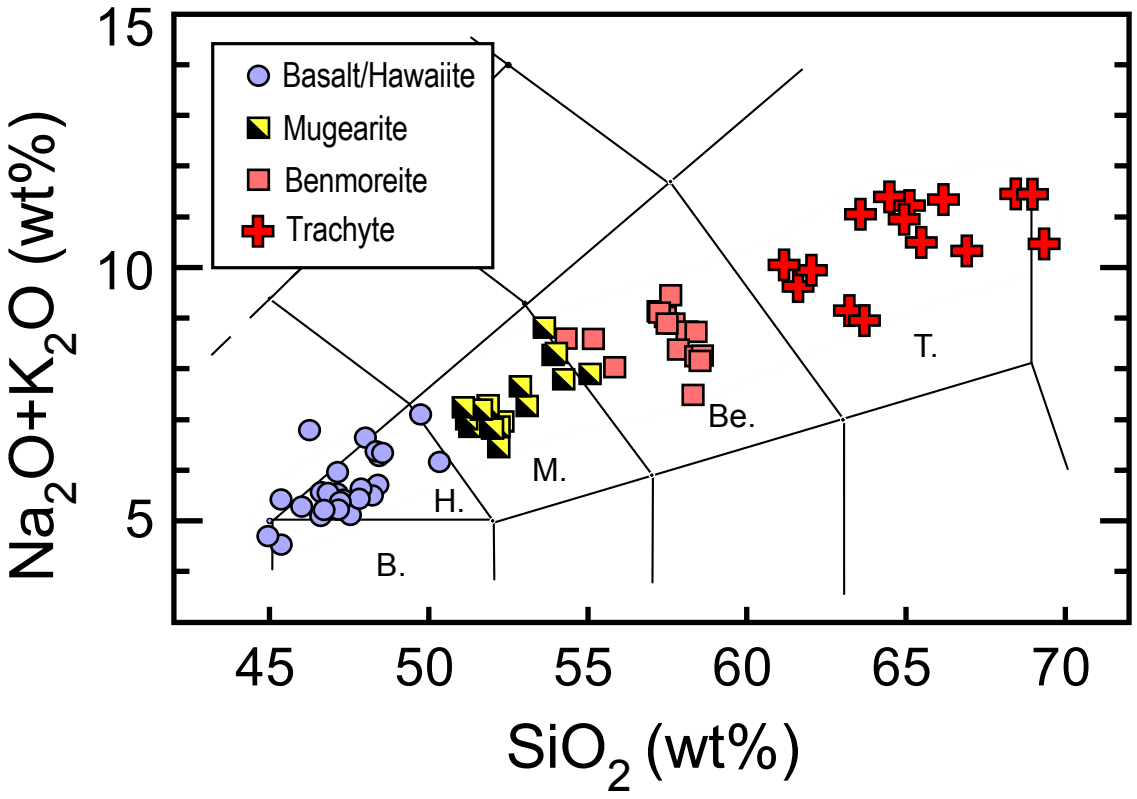

Figure 2: Alkalis versus SiO_2 diagram (supplementary data are from Villemant, 1979). Chaîne des Puys shows a complete compositional range from basalts to trachytes.

Figure 3

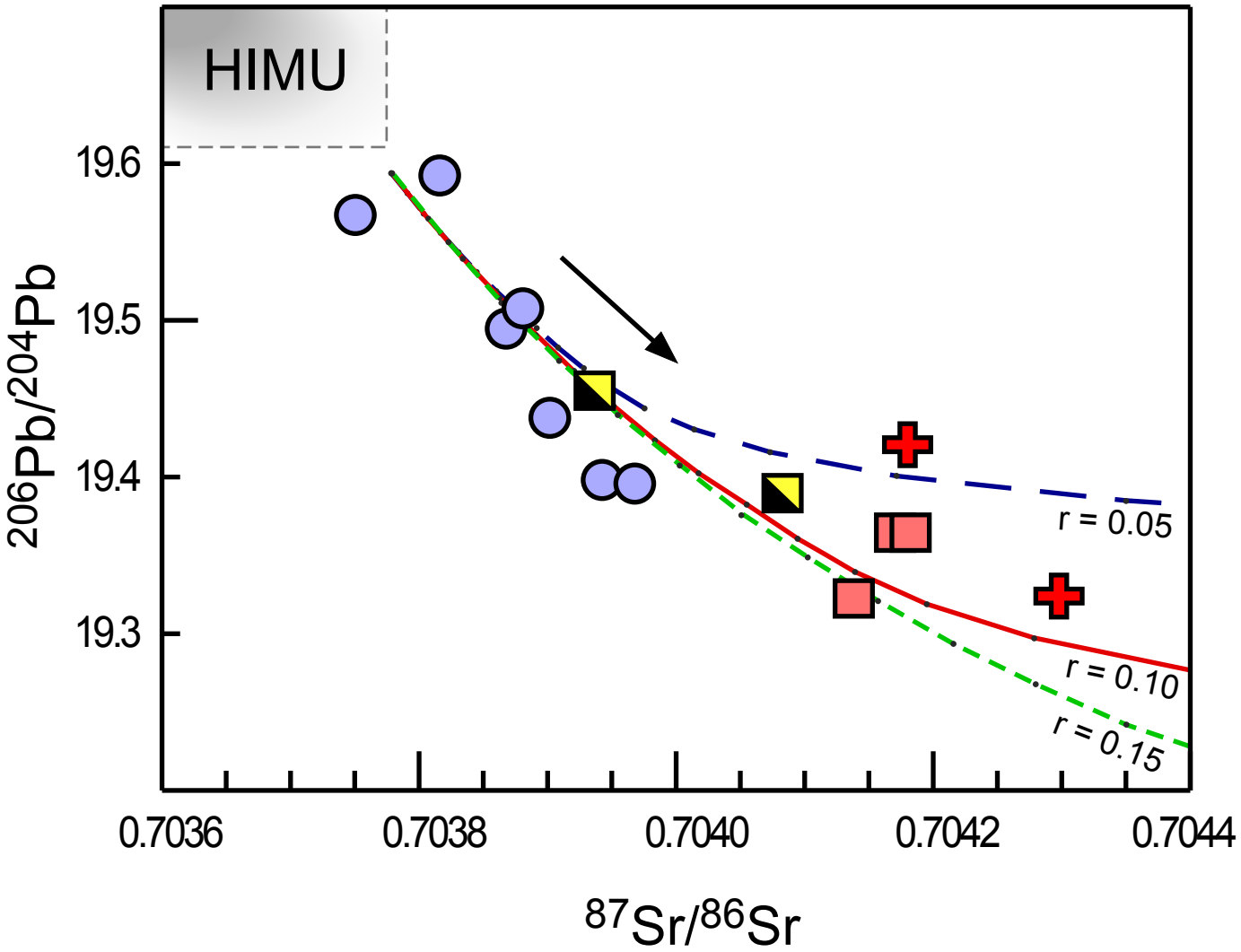

Figure 3: Binary plot of $^{206}Pb/^{204}Pb$ versus $^{87}Sr/^{86}Sr$ (symbols as in Fig. 2). Chaîne des Puys samples are shown superimposed on AFC models, which are calculated using a meta-sedimentary derived lower crustal contaminant and with 3 different values of the ratio between the assimilation and the crystallization mass (r).

Figure 4

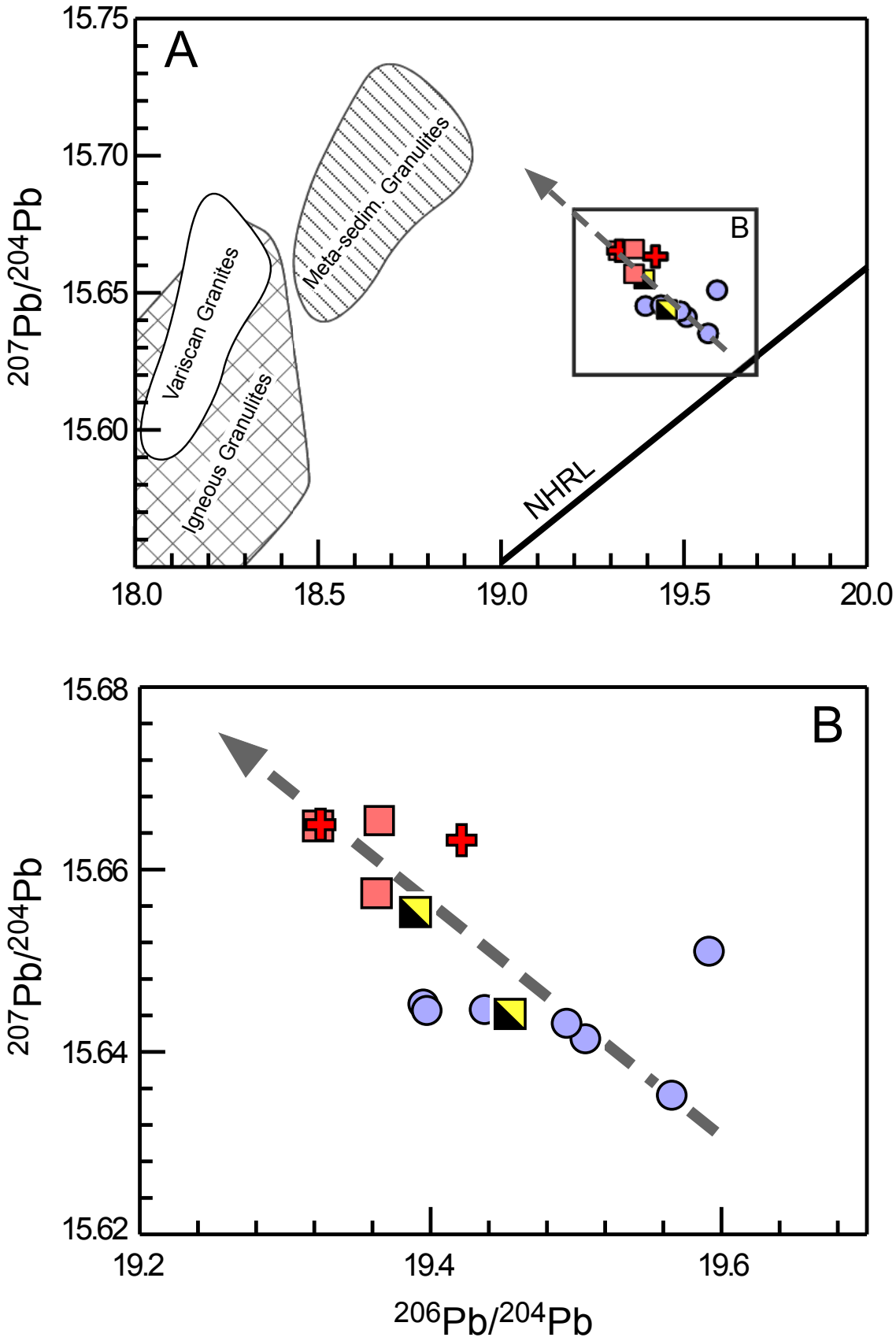

Figure 4: A) Variation of Pb isotopic composition of the Chaîne des Puys series compared to different types of granulites xenoliths exhumed from the lower crust (Downes et al. 1990, 1991) and to upper crustal hercynian granitoïds (Downes et al., 1997). B) zoom on the Pb isotopic variation of the Chaîne des Puys series (symbols as in Fig. 2).

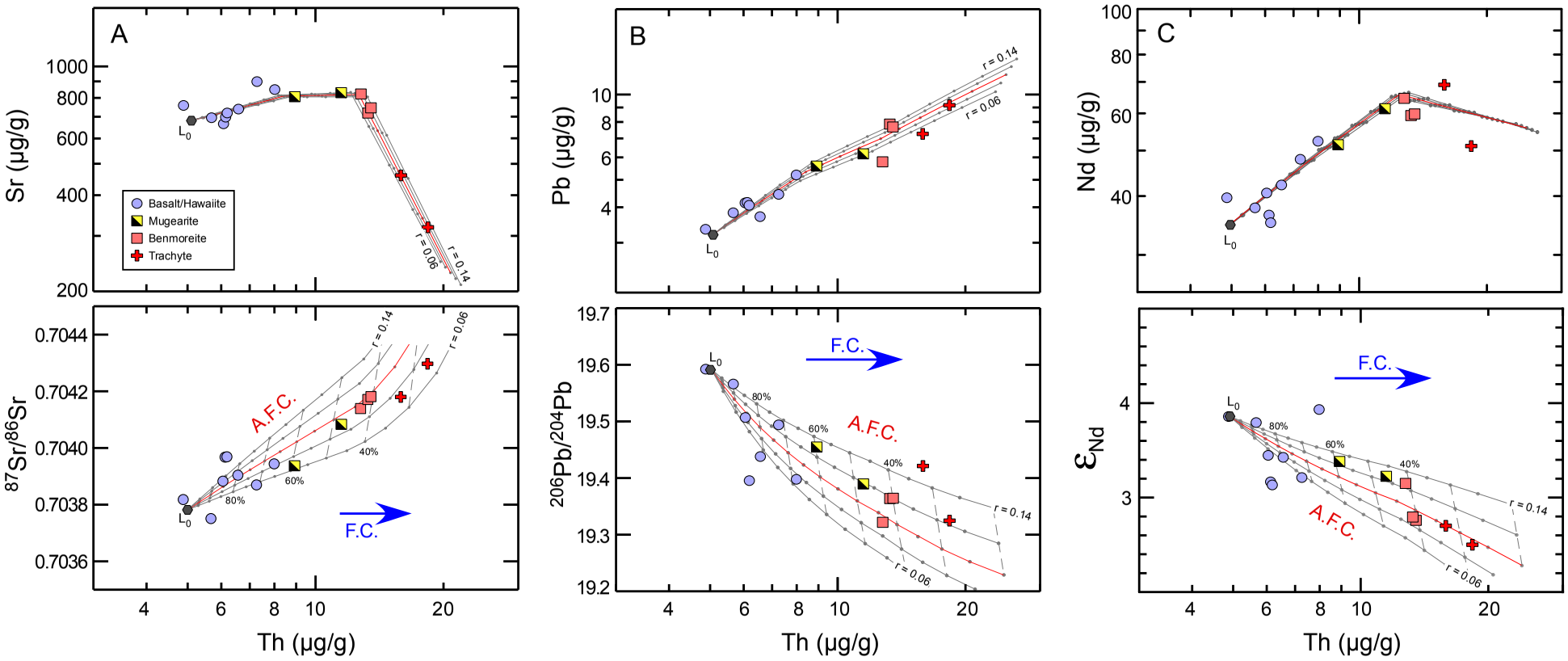

Figure 5a,b,c: Radiogenic isotope compositions plotted vs Th concentration which is used as a differentiation index. AFC models for these systems are shown with different values of the ratio between the assimilation and the crystallization mass: r= 0.06, r= 0.08, r= 0.10, r= 0.12 and r= 0.14. The red line represents our favorite model (r= 0.10). All parameters used for these calculations are in Table 3.

Figure 5

Figure 6

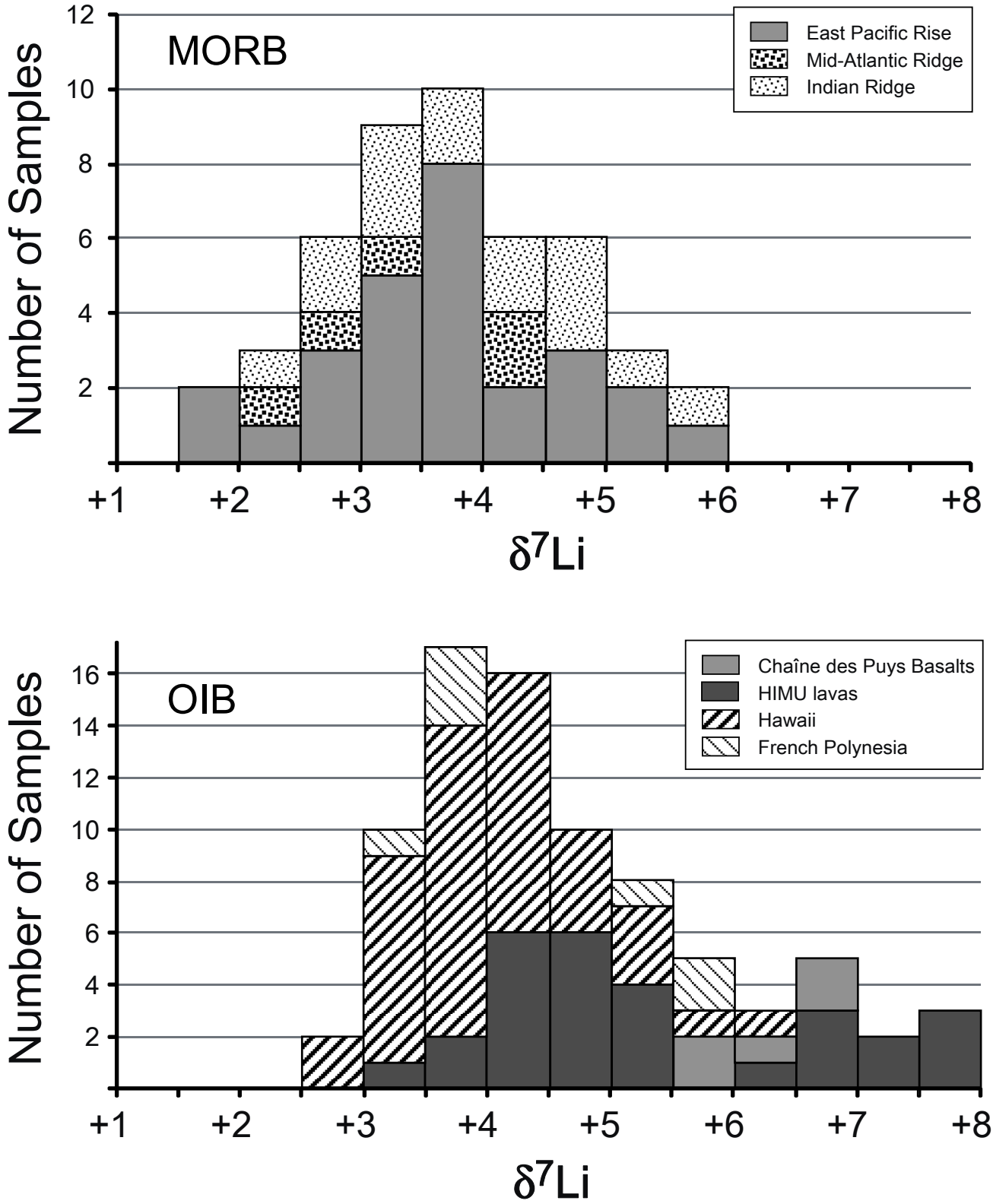

Figure 6: Li isotopes histogram for Mid Oceanic Ridge Basalts (MORB, includes data: Chan et al., 1992; Elliott et al., 2006; Moriguti and Nakamura, 1998; Nishio et al., 2007; Tomascak et al., 2008) and Oceanic Island Basalts (OIB, includes data: Chan and Frey, 2003; Ryan and Kyle, 2004; Nishio et al, 2005; Chan et al., 2009 and basaltic lavas from the Chaîne des Puys).

Figure 7

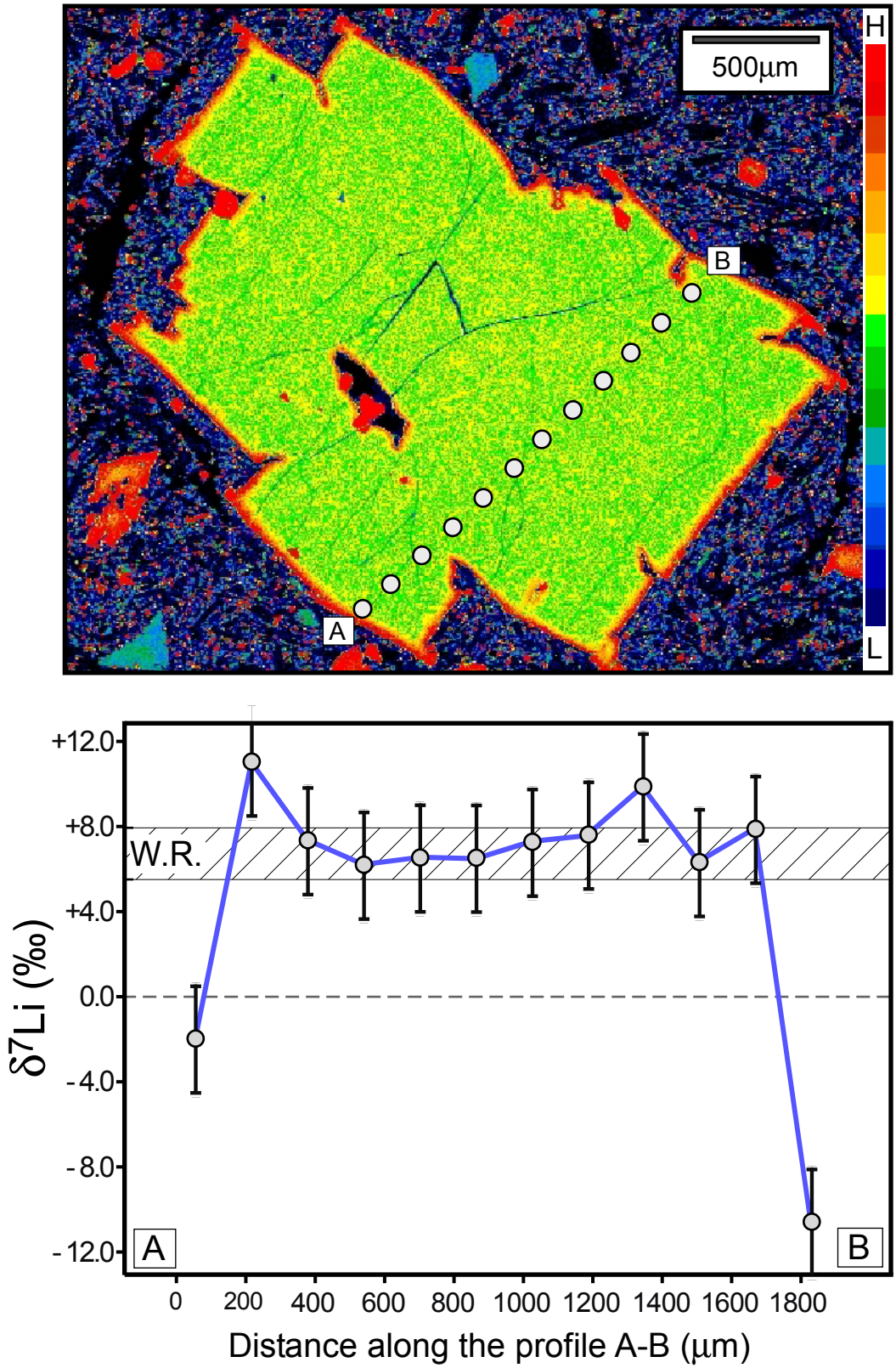

Figure 7: Comparison of whole rock and olivine phenocryst δ^7Li values for the sample Puy 21. Locations of in situ measurements of Li isotopes are shown on a chemical distribution map of Fe.

Figure 8

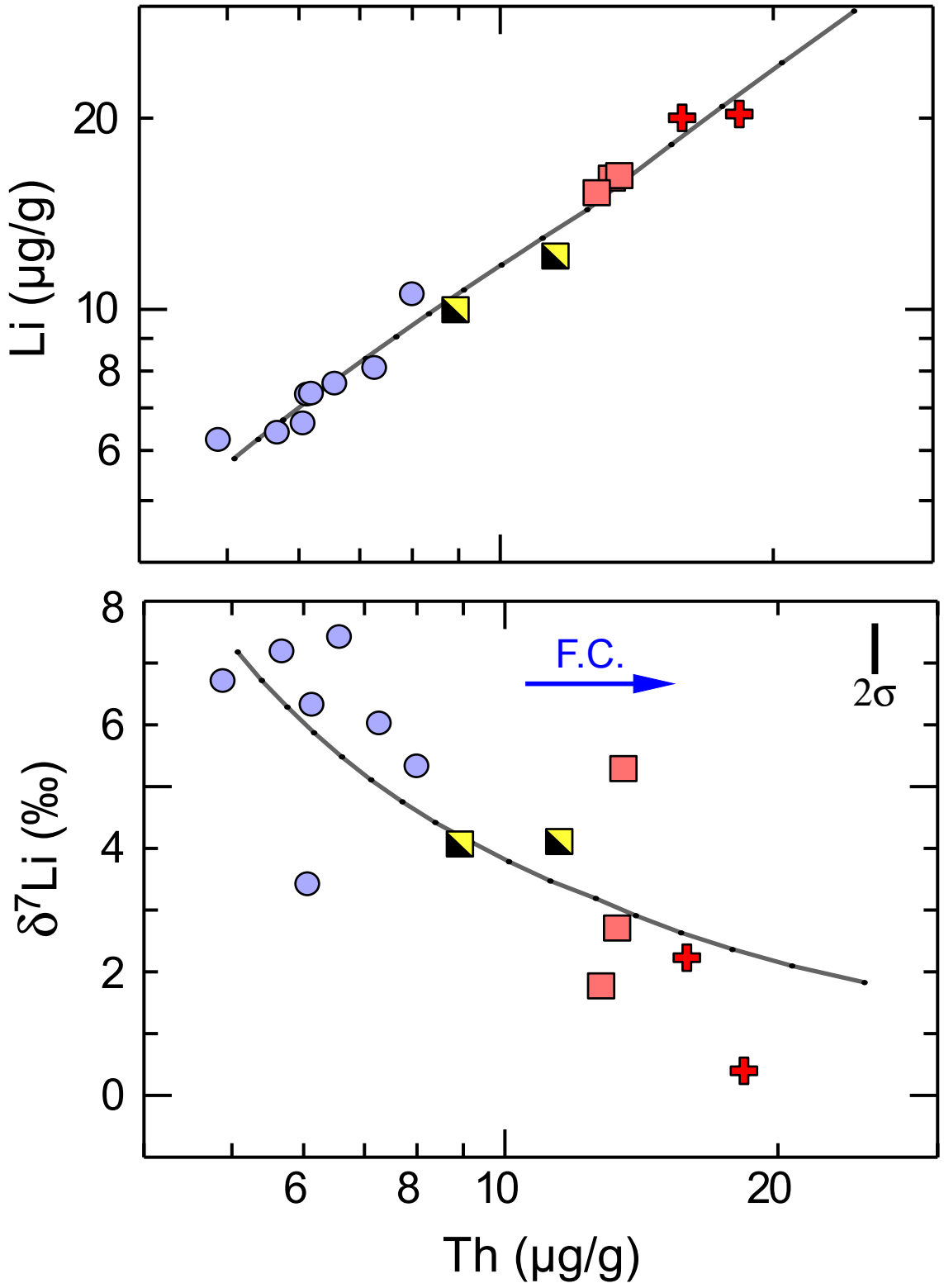

Figure 8: Evolution of Li concentration and isotopic composition along the volcanic suite (symbols as in Fig. 2). The gray line is an example of AFC model showing a minimal residual error. The set of AFC parameters chosen for this model: D_{Li} = 0.3; δ^7Li_c = -5.3‰; $[Li]_c$ = 39.75µg/g; r = 0.10 (see the text and figure 9 for more details).

Figure 9

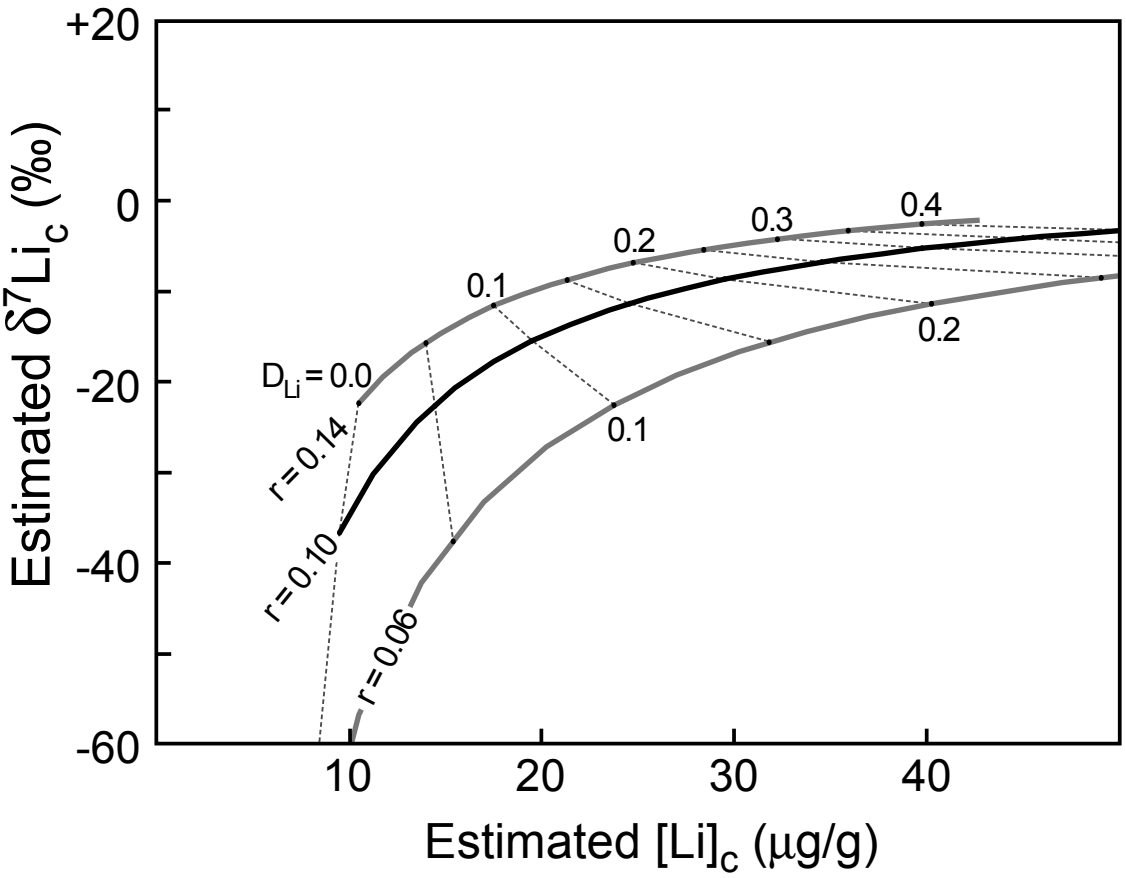

Figure 9: Plot of candidate solutions for the AFC parameters (δ^7Li_c, $[Li]_c$, r and D_{Li}) calculated using an iterative least-squared method. Each solution represents a best-fitting curve of the evolution of the Li abundance and isotopic composition in the Chaîne des Puys volcanic suite. All together, the candidate solutions define the solution space of our model. In this space, our favorite set of AFC parameters is illustrated in figure 8.

Supplementary Figure

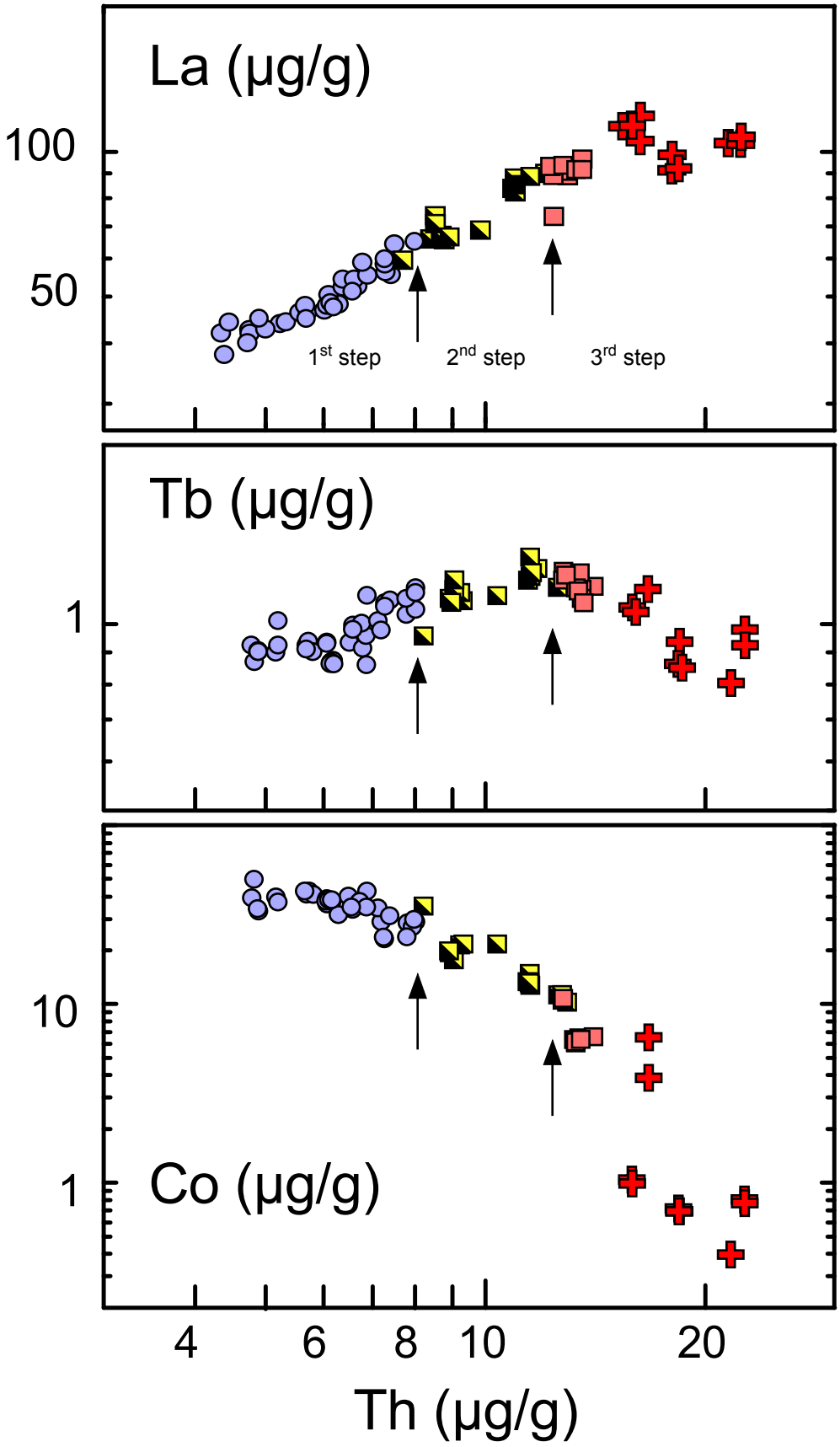

Supplementary Figure: Plot of La, Tb and Co concentrations versus Th concentration, used as a differentiation index (supplementary data are from Villemant (1979)). Arrows point to the important changes due to crystal fractionation. 1st step: plagioclase, clinopyroxene and olivine; 2nd step: plagioclase, clinopyroxene, hornblende, apatite and Fe-Ti oxides. 3rd step: biotite, alkali feldspar, apatite and Fe-Ti oxides.

Table 1: *Major and trace element analyses of Chaîne des Puys samples. BH : basalts and hawaiites; Mu : mugearites; Ben : benmoreites; T : Trachytes.*

	PUY21	**PUY16**	**PUY13**	**PUY20**	**PUY7**	**PUY18**	**PUY1**	**PUY5**
Type	BH	BH	BH	BH	BH	BH	BH	BH
Long (°E)	3°01'39''	3°02'41''	2°59'59''	2°58'20''	2°58'08''	3°03'30''	2°51'39''	2°52'42''
Lat (°N)	45°39'42''	45°52'40''	45°52'32''	45°39'41''	45°44'21''	45°41'31''	45°50'02''	45°47'06''
SiO_2	47.16	46.04	46.61	47.3	47.57	47.22	48.45	48.03
TiO_2	2.4	2.53	2.39	2.29	2.26	2.32	2.07	2.42
Al_2O_3	16.53	16.14	16.76	16.51	15.95	17.35	18.22	17.4
Fe_2O_3	12.13	12.6	12.5	11.94	11.84	12.08	11.51	11.97
MnO	0.19	0.19	0.21	0.18	0.19	0.19	0.21	0.21
MgO	6.3	6.94	6.19	6.45	7.09	5.16	3.77	4.69
CaO	9.83	10.46	9.97	9.67	9.98	9.27	8.62	8.43
Na_2O	3.79	3.57	3.32	3.58	3.44	3.79	4.11	4.48
K_2O	1.77	1.72	1.77	1.86	1.66	1.58	2.17	2.19
P_2O_5	0.66	0.55	0.55	0.56	0.5	0.66	0.8	0.79
L.O.I.	-0.33	-0.42	-0.16	-0.41	-0.01	0.31	0.02	-0.2
Total	100.43	100.32	100.11	99.93	100.47	99.93	99.95	100.41
Mg#	50.7	52.2	49.5	51.7	54.3	45.8	39.3	43.7
Li	6.2	6.4	6.6	7.3	7.4	7.6	8.1	10.5
Be	1.77	1.81	1.92	1.76	1.76	1.94	2.3	2.48
Sc	21.4	27	25.5	25.4	28.2	21.5	12.2	15.5
Co	33.2	41.3	36.3	36.9	36.8	33.8	23.1	28.8
Ni	59.8	76	45.1	73.1	82	31.8	-	24.6
Cu	41.8	57.1	49.1	51.6	55.1	40.5	25.7	37.7
Zn	92	111	107	98	94	101	116	115
Ga	16.9	19.5	19.5	17.8	18.2	19.6	20.5	20.9
Rb	37.6	40.5	48.6	40.8	40.1	55.8	54.4	53.9
Sr	754	691	661	694	717	734	895	845
Y	26.6	26.9	28.9	27.4	26.7	28.5	32.2	34.2
Zr	219	220	237	211	225	240	277	316
Nb	56	66	72	57	70	70	81	90
Ba	510	542	577	574	565	598	660	719
La	44.8	44.7	47.7	48.3	47.2	50.9	59.5	64.6
Ce	90	90	98	90	87	103	118	126
Pr	10.4	10	10.7	10	9.8	11.5	12.8	14
Nd	39.6	37.7	40.5	36.4	35.1	42.2	47.9	52.2
Sm	7.11	7.27	7.65	6.83	6.66	7.98	8.8	9.07
Eu	2.28	2.28	2.33	2.06	2.01	2.43	2.6	2.79
Gd	6.48	6.3	6.24	5.97	5.92	6.68	7.15	7.55
Tb	0.91	0.92	0.94	0.87	0.87	0.99	1.08	1.14
Dy	5.2	5.05	5.36	5.11	4.98	5.36	5.7	6.27
Ho	0.98	0.94	1.01	0.97	0.88	1.01	1.1	1.18
Er	2.51	2.52	2.57	2.51	2.37	2.73	2.9	3.01
Yb	1.92	2.13	2.32	2.11	2.2	2.26	2.59	2.73
Lu	0.29	0.31	0.35	0.31	0.34	0.34	0.39	0.39
Hf	4.85	5.15	5.65	4.77	5.31	5.65	6.15	7.22
Pb	3.34	3.82	4.14	4.15	4.06	3.7	4.43	5.19
Th	4.89	5.68	6.06	6.13	6.19	6.57	7.27	8
U	1.36	1.52	1.56	1.58	1.73	1.64	1.88	2.06

Table 1: *(continued)*

	PUY4	**PUY8**	**PUY9**	**PUY17**	**PUY14**	**PUY11**	**PUY10**
Type	Mu	Mu	Ben	Ben	Ben	T	T
Long (°E)	2°52'05''	3°01'39''	2°59'15''	3°00'21''	3°01'08''	2°57'26''	2°58'56''
Lat (°N)	45°48'31''	45°47'10''	45°48'12''	45°51'38''	45°52'03''	45°45'48''	45°49'05''
SiO_2	51.41	53.88	54.31	57.47	57.21	63.53	64.91
TiO_2	1.89	1.5	1.32	1.09	1.08	0.44	0.42
Al_2O_3	17.85	18.28	18.49	18.55	18.4	17.71	17.67
Fe_2O_3	10.01	8.52	7.78	6.61	6.7	2.85	3.02
MnO	0.22	0.22	0.21	0.21	0.19	0.22	0.21
MgO	3.61	2.62	2.31	1.92	2.01	0.5	0.63
CaO	7.54	6.09	5.27	4.45	4.53	2.04	1.71
Na_2O	4.43	5.25	5.32	5.53	5.6	6.61	6.03
K_2O	2.53	3.04	3.3	3.38	3.53	4.47	4.95
P_2O_5	0.7	0.77	0.72	0.57	0.6	0.18	0.16
L.O.I.	-0.22	0.09	0.95	0.45	0.15	1.47	0.25
Total	99.97	100.26	99.98	100.23	100	100.02	99.96
Mg#	41.7	37.9	37	36.5	37.3	25.8	29.2
Li	10	12.1	15.3	16.1	16.2	20	20.3
Be	2.37	3.35	3.54	3.88	3.83	4.67	4.66
Sc	12.7	8	6.8	5	5.4	2.2	2.1
Co	19.5	12.9	10.6	6.1	6.3	1	0.7
Ni	22	10.8	8.5	5.7	6.2	-	-
Cu	25.8	16.8	14.1	11.9	11.8	6.2	4.8
Zn	99	110	106	95	97	108	71
Ga	20.1	21.3	22.2	20.1	20.5	20	20.3
Rb	54.7	81.4	86.4	96.7	90.7	127.6	133.5
Sr	803	825	819	715	742	458	317
Y	33.4	37.4	38.1	36	36.9	31.5	29.5
Zr	332	431	454	466	500	702	701
Nb	107	120	123	115	135	177	178
Ba	754	950	1026	1038	1037	1410	1184
La	66.2	88.1	93.1	91.1	91.3	112.3	91.4
Ce	131	161	180	163	171	211	176
Pr	14.3	17.4	18.4	17.7	17.5	21.1	16.5
Nd	51.5	61.4	64.6	59.3	59.9	68.9	51
Sm	9.1	10.37	10.68	9.67	9.82	10.31	7.78
Eu	2.7	2.86	2.95	2.62	2.75	2.6	1.89
Gd	7.25	8.4	8.25	7.76	7.65	7.18	5.29
Tb	1.1	1.23	1.22	1.15	1.1	1.06	0.86
Dy	6.14	6.79	6.8	6.07	6.34	5.67	5.06
Ho	1.18	1.26	1.28	1.18	1.2	1.11	0.95
Er	2.94	3.37	3.33	3.42	3.31	3.29	2.7
Yb	2.87	3.24	3.38	3.22	3.25	3.61	3.03
Lu	0.42	0.48	0.52	0.47	0.5	0.59	0.45
Hf	7.49	9.02	9.78	10.22	10.76	12.85	12.89
Pb	5.58	6.18	5.78	7.86	7.68	7.26	9.16
Th	8.92	11.5	12.77	13.28	13.51	15.87	18.35
U	2.22	3.06	3.31	3.49	3.54	4.18	4.85

Table 2: concentration (ppm) and isotopic composition of Sr, Nd, Pb and Li for the Chaîne des Puys volcanic rocks. BH : basalts and hawaiites; Mu : mugearites; Ben : benmoreites; T : Trachytes. Uncertainty is the 2σ standard deviation.

	Th	Sr	Pb	Nd	Li	$^{87}Sr/^{86}Sr$	$^{143}Nd/^{144}Nd$	ε_{Nd}	$^{206}Pb/^{204}Pb$	$^{207}Pb/^{204}Pb$	$^{208}Pb/^{204}Pb$	$\delta^{7}Li$
PUY21 (BH)	4.9	754	3.34	39.6	6.2	0.703817±7	0.512835±8	+ 3.85	19.592	15.651	39.563	+6.7 ±0.2
PUY16 (BH)	5.7	691	3.82	37.7	6.4	0.703750±7	0.512832±6	+ 3.79	19.566	15.635	39.519	+7.2 ±1.2
PUY13 (BH)	6.0	661	4.14	40.5	6.6	0.703882±7	0.512814±5	+ 3.44	19.507	15.641	39.493	+3.4 ±1.2
PUY20 (BH)	6.1	694	4.15	36.4	7.3	0.703967±7	0.512800±8	+ 3.17	-	-	-	+6.3 ±0.9
PUY7 (BH)	6.2	717	4.06	35.1	7.4	0.703968±6	0.512798±8	+ 3.13	19.395	15.645	39.405	-
PUY18 (BH)	6.6	734	3.70	42.2	7.6	0.703903±7	0.512813±6	+ 3.42	19.437	15.645	39.478	+7.4 ±1.1
PUY1 (BH)	7.3	895	4.43	47.9	8.1	0.703869±7	0.512802±9	+ 3.21	19.494	15.643	39.501	+6.0 ±1.1
PUY5 (BH)	8.0	845	5.19	52.2	10.5	0.703943±7	0.512839±8	+ 3.93	19.398	15.645	39.384	+5.3 ±1.1
PUY4 (Mu)	8.9	803	5.58	51.5	10.0	0.703937±8	0.512811±8	+ 3.38	19.455	15.644	39.494	+4.1 ±0.5
PUY8 (Mu)	11.5	825	6.18	61.4	12.1	0.704083±6	0.512803±8	+ 3.23	19.389	15.655	39.402	+4.1 ±1.0
PUY9 (Ben)	12.8	819	5.78	64.6	15.3	0.704139±7	0.512799±6	+ 3.15	19.322	15.665	39.536	+1.8 ±0.6
PUY17 (Ben)	13.3	715	7.86	59.3	16.1	0.704171±7	0.512781±7	+ 2.8	19.364	15.657	39.387	+2.7 ±0.6
PUY14 (Ben)	13.5	742	7.68	59.9	16.2	0.704181±7	0.512779±8	+ 2.76	19.364	15.665	39.400	+5.3 ±0.8
PUY11 (Tr)	15.9	458	7.26	68.9	20.0	0.704180±8	0.512776±8	+ 2.70	19.421	15.663	39.472	+2.2 ±1.0
PUY10 (Tr)	18.3	317	9.16	51.0	20.3	0.704297±7	0.512766±8	+ 2.50	19.324	15.665	39.398	+0.4 ±0.7

Table 3a: Bulk distribution coefficients for Sr and Nd as calculated from log-log diagrams.

	D (1st step)	D (2nd Step)	D (3rd Step)
Sr	0.57	0.9	2.9
Nd	0.25	0.35	1.1
Pb	0.23	0.5	0.5
Th	0	0	0,2

Table 3b: Composition of the components used for the AFC calculations. The geochemical characteristics of the crustal component are an average of meta-sedimentary xenoliths (Downes et al., 1990; 1991).

	Initial Liquid	Crustal contaminant
Sr	680	236
Nd	35	32.4
Pb	3.2	16
Th	5.1	9.6
$^{87}Sr/^{86}Sr$	0.70378	0.71717
$^{143}Nd/^{144}Nd$	+3.84	-11.3
$^{206}Pb/^{204}Pb$	19.59	18.60
$^{207}Pb/^{204}Pb$	15.64	15.67
$^{208}Pb/^{204}Pb$	39.52	38.99

Table 3c: two different models used to obtain the best fit for the Li system (see text for more details).

	model 1	model 2
D_{Li}	0	0.3
$[Li]_c$ (ppm)	10	40
δ^7Li_c (‰)	-50	-9